Environmental Earth Sciences (2021) 80:528
https://doi.org/10.1007/s12665-021-09877-z

ORIGINAL ARTICLE

Distribution for hydraulic head on tunnel structures in water-rich mountainous region considering influences of fault geology using virtual image technique

Zhiguo Zhang[1,2,3,4] · Mengxi Zhang[5] · Zhenbo Li[1] · Qihua Zhao[4] · Yutao Pan[3,6] · Jiacheng Wang[1] · Zhongteng Wu[2]

Received: 11 September 2020 / Accepted: 1 August 2021 / Published online: 10 August 2021

Abstract

Tunnel excavation in mountainous region frequently encounters high local inflows as a consequence of hydraulic head and multiple faults geology, which may adversely affect the serviceability of tunnel structures. Previous researches, however, paid very little attention to the seepage field of rocks around deep buried tunnels adjacent to water-bearing faults under high hydraulic head. In this paper, a new close-form analytical method is proposed to investigate the combined effect of high far-field hydraulic head and head generated by water-bearing faults on mountain tunnel structures. First, the virtual image technique and conformal mapping theory are employed to evaluate the water discharge and the head variation at concerned locations of deep circular tunnel embedded in water-rich zone, such as the lining, grouting ring and surrounding rocks. Second, the head difference is introduced as a new parameter to predict the uneven distribution of hydraulic head on tunnel structures. Then this paper contrasts to the classical Harr analytical solution and implements numerical simulation on the fault geological conditions to examine the presented analytical method, receiving reasonable agreements. Furthermore, sensitivity analyses are preformed to investigate the performance of concerned parameters on the distribution of hydraulic head on tunnel structure adjacent to water-bearing fault, including the magnitude of head induced by water-bearing fault, spacing between fault and tunnel, water discharge after drainage ditch installed and fault dip. The interesting point and ingenious approach are tracing the corresponding analytic functions for not only the influence of vertical fault adjacent to the tunnel but also the fault with an inclined angle, which enhances the engineering applicability of presented method. In general, this work contributes to the preliminary design of tunnels in water-rich fault zones and provides a theoretical basis on the tunnel excavation and operation in the mountainous area and other adverse geological environments with faults.

Keywords Deep tunnel · Water-bearing fault · Tunnel–fault interaction with inclined angle · Seepage field · Conformal mapping · Virtual image technique

List of symbols

α	Coefficient
λ	Modified function
ρ_1, ρ_2	Distance from observation point to pumping well and injection well
Φ	Potential function
Φ_1, Φ_2	Potential function of pumping well and injection well
Φ_c	Potential at the fault boundary
$\overline{\Phi}$	Modified potential function

✉ Zhiguo Zhang
zgzhang@usst.edu.cn; ceev217@nus.edu.sg

[1] School of Environment and Architecture, University of Shanghai for Science and Technology, 516 Jungong Road, Shanghai 200093, China

[2] Key Laboratory of Geohazard Prevention of Hilly Mountains (Ministry of Natural Resources), Fujian Key Laboratory of Geohazard Prevention, Fujian 350002, China

[3] Department of Civil and Environmental Engineering, National University of Singapore, Singapore, Singapore

[4] State Key Laboratory of Geohazard Prevention and Geoenvironment Protection, Chengdu University of Technology, Chengdu 610059, Sichuan, China

[5] School of Mechanics and Engineering Science, Shanghai University, Shanghai 200444, China

[6] Faculty of Engineering, Norwegian University of Science and Technology, Trondheim, Norway

$\overline{\Phi}_{sl}$, $\overline{\Phi}_{fl}$, $\overline{\Phi}_{g}$, $\overline{\Phi}_{r}$	Modified potential function in secondary lining, primary lining, grouting ring and surrounding rock
φ	Potential function
ω	Mapping function
a, b, a', b'	Coefficients
$A(r)$	Cross-sectional area of the seepage
C_1, C_2	Integration constants
C_u	Constant
d	Distance between the tunnel centerline and water-bearing fault
h	Water head
h_1, h_2, h_3	Water head at the boundary between secondary lining and primary lining, between primary lining and grouting ring, and between grouting ring and surrounding rock
h_r	Water head in the surrounding rock
h_p	Pressure head
h'_1, h'_2, h'_3	Water head at the boundary between secondary lining and primary lining, between primary lining and grouting ring, and between grouting ring and surrounding rock induced by fault head
h_{1w}, h_{2w}, h_{3w}	Water head at the boundary between secondary lining and primary lining, between primary lining and grouting ring, and between grouting ring and surrounding rock induced by far-field head
h_{sl}, h_{fl}, h_g, h_r	Water head in the secondary lining, primary lining, grouting ring and surrounding rock
h_{slw}, h_{flw}, h_{gw}, h_{rw}	Water head in secondary lining, primary lining, grouting ring and surrounding rock induced by far-field head
H_f	Water-bearing fault head
H_w	Far-field head
k	Permeability coefficient
k_1, k_2, k_3, k_4	Permeability coefficient of secondary lining, primary lining, grouting ring and surrounding rock
$\overline{k}$	Equivalent permeability coefficient
L_0, L_1, L_2, L_3, L_4	Boundary of secondary lining, between secondary lining and primary lining, between primary lining and grouting ring, boundary between grouting ring and surrounding rock, and surrounding rock
m	Constant
Q	Total water discharge
Q_f	Water discharge induced by water-bearing fault
Q_w	Water discharge induced by far-field head
r	Radius of radial seepage
r_0	Inner radius of tunnel
$r_1r_2r_3$	Radius of secondary lining, primary lining and grouting ring
R	Radius of far field
v	Seepage velocity
v_1, v_2, v_3, v_4	Seepage velocity in secondary lining, primary lining, grouting ring and surrounding rock
V	Rradial seepage velocity
x,y	Coordinates

Introduction

At present, the world has entered an accelerating period of the urbanization. Owing to the rapid growth of urban population, the numerous operative infrastructures have sprung up extensively in rural and remote areas to relieve the traffic congestion in large cities. As an efficient means of transportation, mountain tunnels have been widely constructed to traverse natural obstacles and cut through rock mass with disparate properties and depths (Ye et al. 2012; Kargar et al. 2020). However, the mountain tunnel excavation is still a challenging task that requires full risk assessments in early stage. In spite of practical experiences in tunnel constructions (Ikuma 2005; Xie et al. 2013; Kargar et al. 2019), yet the design of mountain tunnel is confronted with unforeseeable high risks (Miura 2003; Boultbee et al. 2018; Deng 2018; Lai et al. 2018; Zhu et al. 2019), which stem from geological uncertainties, e.g., fault, groundwater, high geo-stress and temperature, and earthquake (Nam and Bobet 2006; Luo et al. 2008; Bian et al. 2009; Zhao et al. 2013; Lin et al. 2014; Shen et al. 2014; Liu et al. 2015; Dong et al. 2018a; Wu et al. 2018; Zhang et al. 2018a, b; Lyh et al. 2020), which have detrimental effects on tunnels if treated inappropriately. Therefore, more attention should be aroused for the sophisticated environments faced in the course of mountain tunnel construction. In addition, there are high chances that mountain tunnels encounter a high hydraulic head in water-rich mountainous region in the tunnel construction and operation, causing problems, such as water leakage and lining collapse (Cheng et al. 2019). For tunnels buried in water-rich region, there is strong possibility that the tunnel lining is subjected to an enormous water pressure induced by the groundwater. Therefore, grouting circle is applied to tunnel construction as a geotechnical improvement technique to ensure construction safety and reduce water inflow (Lee et al. 2004). Nevertheless, in practical

engineering, numerous mountain tunnels may traverse or be adjacent to faults, easily vulnerable to be destructed. Moreover, it may occur the fault in water-rich zone, which is filled with water, named water-bearing fault. The head of the fault will have effect on the initial seepage field generated by groundwater and may destroy the existing tunnel structure. Consequently, the urgent problem to be solved is how to accurately determine the head distribution on the key structure of the tunnel under the influences of water-bearing fault geology, which can evaluate the pressure on the tunnel structure to avoid the occurrence of earlier damage (Bobet 2003; Moon and Jeong 2010).

With regard to the recent attempts to develop the solutions for external water pressure of lining under high hydraulic head, the methods are divided into four categories: namely, empirical methods (Vaughan 1956; Patterson et al. 1957; Young and Falkiner 1966; Zagars 1982), analytical solutions (Harr 1962; Snow 1969; Hwang and Lu 2007; Kolymabas and Wagner 2007; Park and Lee 2008; Arjoni et al. 2009; Fahimifar and Zareifard 2009; Li and Low 2010; Huang et al. 2015; Kargar et al. 2015; Wu et al. 2017; Tan et al. 2018; Wu et al. 2019), numerical simulations (Lee and Nam 2004; Yoo 2005; Shin et al. 2005, 2009; Lee et al. 2007; Fernandez and Moon 2010; Yu et al. 2013), and physical model tests (Wang et al. 2008; Fang et al. 2016). Generally speaking, the empirical method is closely tied to field observations and intuitive deductions, which lead to lack of theoretical basis and applicability. The seepage field needs to be analyzed in detail for tunnels with sophisticated surrounding rock conditions. With respect to the complex soil behavior and geometric conditions, the numerical simulation provides effective support to approximate the seepage field. Shin et al. (2009) put forth the variation law of lining water pressure under different drainage patterns via numerical model. The numerical simulation can establish the engineering practice, considering the influence of various factors on the tunnel lining water pressure. However, even though the numerical simulation is extremely helpful, the surrounding rock is generally simplified as isotropic continuous medium, which is not consistent with the actual rock characteristics. In addition, the numerical simulation consumes high costs and lots of time in modeling and computing. Especially for different engineering cases of geometry and boundary, such as the thickness of tunnel lining, the distance between tunnel and fault, and so on, the simulation modelling has been built once more. However, the analytical closed-form method is consistently favored for its explicit theoretical derivations in determining external water pressure of lining on the basis of the seepage theory, by means of simplifying the surrounding circumstances of the tunnel to establish a suitable calculation model. Harr (1962) employed the virtual image method and superposition principle for analytically predicting the seepage field distribution of the deep buried tunnel in high head region. Kolymabas and Wagner (2007) established a mathematical model in the light of the conformal transformation theory to propose the calculation method of the external water pressure of the tunnel structure under the condition of stable hydrologic seepage. Fahimifar and Zareifard (2009) presented the calculation formula of the external water pressure of the lining structure with consideration of fluid–structure interaction. Kargar et al. (2015) proposed a complex variable solution to investigate stress components around non-circular hydraulic tunnels considering the effects of groundwater and internal water pressure. Wu et al. (2017) studied the flow characteristics and escape-route optimization after water inrush in a backward-excavated karst tunnel. Tan et al. (2018) extended the existing analysis model of tunnel lining water flow under steady and saturated conditions. Wu et al. (2019) developed generalized models and computational techniques to estimate the required thickness of supporting rock stratum to prevent water and mud inrush under earthquake action. Dong et al. (2019) obtained the stress distribution in deep lined tunnels under the water table using the complex variable method and the conformal mapping technique. Dong et al. (2020) extended their contribution on the stress and energy redistribution in arbitrarily shaped openings upon excavation by taking into account the effect of fluid flow (Dong et al. 2018b). For the actual project engineering is generally more complicated, the solutions derived from theoretical analysis should be improved to satisfy the application of practical engineering to a certain extent, such as the influences of fault geology should be further considered.

Currently, multitudinous scholars have conducted a deep research on the seepage field of tunnel in high hydraulic head region. Nevertheless, the tunnel in the mountainous region with high hydraulic head will inevitably encounter the influence of faults. The existing study on the adjacent fault tunnels is mostly focused on the stability of surrounding rock, while there is a shortage of available researches that can adequately describe the seepage field of the water-bearing fault (Jeon et al. 2004; Childs et al. 2009; Zhang et al. 2017). Kim et al. (2011) proposed a case study to investigate the collapse and reinforcement for large span waterway tunnel at thrust fault zone. Zhao et al. (2014) employed a 3D numerical simulation based on site investigation to deal with these severe geotechnical problems encountered when tunnelling through a fault zone. Wang et al. (2016a, 2016b) established a three-dimensional numerical model to simulate the dynamic processes of tunnel excavation through the fault fracture zone. Zhang et al. (2018a, b) presented a case history of geological hazards and treatment measures during the shield tunneling of Metro Line No. 7, in water-rich mylonitic faults in Guangzhou, China. Zhao et al. (2019) conducted the mechanical tests to prevent damage to tunnel lining caused by fault movement using the fibre plastic

concrete. Huang et al. (2020) investigated the failure mechanism of a tunnel in the vicinity of a fault zone by physical model tests and the results show that the fault zone near the tunnel shoulder has a significant influence on the stability of the surrounding rock. The above achievements for analytical mechanical researches of tunnel-fault interaction have important implications (Kim et al. 2011; Zhao et al. 2014, 2019; Wang et al. 2016a, b; Zhang et al. 2018a, b; Huang et al. 2020).

As a consequence for obtain the distinct mechanics and simplified design sketch, this paper concentrates on the problem stemming from actual tunnels in Niuheling tunnel in Zhejiang Province, China, and introduces an analytical method of deep buried circular tunnel for seepage field at concerned locations as the lining, grouting ring and surrounding rock under a combined interaction of a far-field head and a water-bearing fault head. Unlike the existing researches, this work investigates not only the influence of vertical fault adjacent to the tunnel but also the fault with an inclined dip, which enhances the applicability of the presented method. In the first place, this paper acquires the tunnel water discharge under the action of seepage between far-field head and water-bearing fault head in the light of the seepage theory and complex variable method. Then, the pressure head at the tunnel structure is obtained by the virtual image method after the superposition of the discharge. Besides, both the established related models and the existing Harr solutions (Harr 1962) are conducted to verify the reliability and accuracy of the analytical solutions. Finally, a number of concerned parameters are discussed, namely, magnitude of head on water-bearing fault, distance between fault and tunnel, water discharge, and fault dip, which may supply the references for practical engineering henceforth.

Water discharge of tunnel adjacent to water-bearing faults

Basic assumptions of mechanical model

In an attempt to acquire the water discharge, this paper establishes the following assumptions according to the seepage characteristics of deep buried mountain tunnel under a high hydraulic head before the lining drainage ditch is installed: (1) the surrounding rock is isotropic and homogeneous and is considered as continuous medium; (2) the groundwater is incompressible and strictly follow the pattern of steady seepage; (3) the tunnel discharge is viewed as the superposition of discharge under the seepage action of far-field head water-bearing fault head; and (4) the heads at the interface of the primary lining, secondary lining and surrounding rock are regarded equal in the single analysis of the far-field seepage or fault seepage.

The assumption (4) is based on research (Liu 2012) on solving the drainage of tunnel lining under the action of water head in the far field. The results show a high accuracy on comparison with the actual monitoring data. In this study, when calculating the tunnel drainage under the action of the far-field head and the water-bearing fault head in this project, however, there is a big error between the theoretical data and the extracted actual monitoring data of the drainage. The values of drainage using analytical method is relatively small. Therefore, considering the influence of the water-bearing fault head, the seepage influence analysis of the water head of the water-bearing fault is introduced. The results show that the superposition of the drainage action of far-field water head and the fault head is close to the actual values of Niuheling tunnel. The comparative results are shown in Table 1. Five sections have been selected to calculate the drainage of tunnel including sections A, B, C, D, and E as listed in Table 1.

As mentioned above, the tunnel discharge can be resolved by dividing the tunnel seepage into two parts: the far-field seepage and the fault seepage. The seepage model is revealed in Fig. 1, in which the far-field head and the head at the boundary of the water-bearing fault are defined as H_w and H_f. Moreover, the circular rings inside the tunnel represent the secondary lining, primary lining and grouting ring from inside to outside.

The water discharges of the far-field head and the water-bearing fault head are defined as Q_w and Q_f, respectively. Therefore, the total seepage discharge can be written as

$$Q = Q_w + Q_f. \tag{1}$$

Water discharge induced by far-field head

In reality, the water head in the surrounding rock will be remarkably decreased owing to the tunnel excavation. However, the influence of construction on surrounding rock seepage will only be reflected in a certain circular area,

Table 1 Comparison of drainage results of Niuheling Tunnel (Per linear meter)

	Monitoring drainage (m^2/d)	Not consider the effect of fault head		Consider the effect of fault head	
		Drainge (m^2/d)	Error	Drainge (m^2/d)	Error
Section A	1.76	1.03	41.5%	1.92	8.0%
Section B	3.53	2.66	24.6%	3.27	7.4%
Section C	3.44	2.46	28.5%	3.24	5.8%
Section D	1.60	1.12	30.0%	1.75	9.4%
Section E	2.37	1.92	19.0%	2.22	6.3%

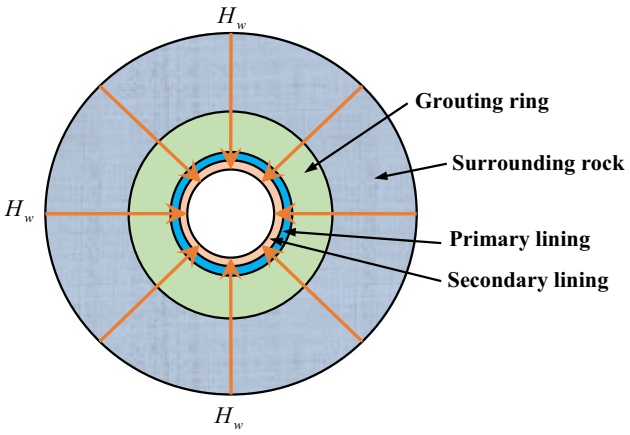

(a) Far-field seepage

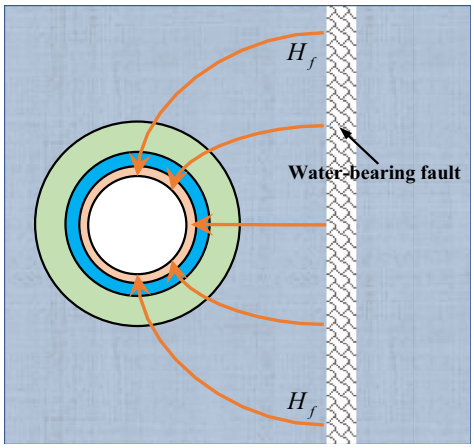

(b) Fault seepage

Fig. 1 Simplified model of seepage in tunnel engineering. (**a**) Far-field seepage. (**b**) Fault seepage

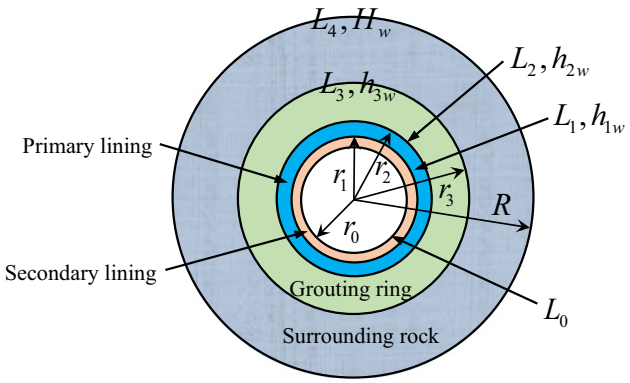

Fig. 2 Calculation model of far-field head

considering the tunnel in an infinite area. The radius of the circular area is defined as the far-field radius, and so as the head on the far-field radius named as far-field head. The analytical model of the far-field head seepage is shown in Fig. 2. When only the far-field water head seepage is taken into account, the tunnel area is divided into four parts from inside to outside: the secondary lining, primary lining, grouting ring and surrounding rock. The boundaries of the five circles are remarked by L_0, L_1, L_2, L_3, L_4 from inside to outside, and the related radii are r_0, r_1, r_2, r_3, R, respectively. It is identical with the heads on each curve, which are 0, h_{1w}, h_{2w}, h_{3w}, H_w, respectively. The far-field boundary curve L_4 is the circular far-field boundary of surrounding rock, and the corresponding radius R and water head H_w can be acquired according to the project data.

In the analysis of the tunnel discharge induced by far-field head seepage, the influence of the tunnel excavation on the seepage is not taken into account. Therefore, the seepage differential equation in the polar coordinates can be expressed as

$$\frac{\partial^2 h}{\partial r^2} + \frac{1}{r}\frac{\partial h}{\partial r} = 0, \tag{2}$$

where h is the hydraulic head and r is the radial seepage radius.

The general solution of Eq. (2) can be derived as

$$h = C_1 + C_2 \ln r, \tag{3}$$

where C_1 and C_2 are constants of the integration.

The head distribution on the area can be calculated by substituting the boundary conditions of water pressure in each area in the plane, as follows:

(1) In the second lining $(r_0 \le r \le r_1)$, the pressure head at the boundary L_0 is 0 and that at L_1 is h_{1w}. Therefore, the head distribution in the secondary lining can be obtained as

$$h_{slw} = \left(\ln \frac{r}{r_0} / \ln \frac{r_1}{r_0}\right) h_{1w}. \tag{4}$$

(2) In the primary lining $(r_0 \le r \le r_1)$, the pressure head at the boundary L_1 and L_2 are h_{1w} and h_{2w}, respectively. Then, the head distribution in the secondary lining can be written as

$$h_{flw} = \left(h_{1w} \ln \frac{r_2}{r} + h_{2w} \ln \frac{r}{r_1}\right) / \ln \frac{r_2}{r_1}. \tag{5}$$

(3) Similarly, the distribution in the grouting ring $(r_2 \le r \le r_3)$ and surrounding rock $(r_3 \le r \le R)$ are displayed in Eqs. (6) and (7):

$$h_{gw} = \left(h_{2w} \ln \frac{r_3}{r} + h_{3w} \ln \frac{r}{r_2}\right) / \ln \frac{r_3}{r_2} \tag{6}$$

$$h_{rw} = \left(h_{3w} \ln \frac{R}{r} + H_w \ln \frac{r}{r_3} \right) / \ln \frac{R}{r_3}. \tag{7}$$

In Eqs. (4–7), the value of far-field head H_w can be checked from related geological reports, and h_{1w}, h_{2w}, h_{3w} are all unknown variables. Accordingly, it can be carried out to combine the continuous condition of seepage velocity at the boundary of two adjacent zones and the relationship between seepage velocity and hydraulic head.

The continuous conditions of seepage are exhibited as follows:

$$\begin{cases} v_1|_{r=r_1} = v_2|_{r=r_1} \\ v_2|_{r=r_2} = v_3|_{r=r_2} \\ v_3|_{r=r_3} = v_4|_{r=r_3} \end{cases}, \tag{8}$$

where v_1, v_2, v_3, v_4 are seepage velocities in the secondary lining, primary lining, grouting ring and surrounding rock, respectively.

In the light of the Darcy's law and the derivation of Appendix A, the relationship between seepage velocity and hydraulic head is expressed as

$$v = -k \frac{\partial h}{\partial r}, \tag{9}$$

in which k is the permeability coefficient, and the coefficients of the secondary lining, primary lining, grouting ring and surrounding rock are denoted by k_1, k_2, k_3, k_4, respectively.

Combining Eqs. (4–9), the head of each position indicated by the far-field head can be obtained, and then substitute it in the expression of each head distribution. The distribution in the secondary lining $(r_0 \le r \le r_1)$, primary lining $(r_1 \le r \le r_2)$, grouting ring $(r_2 \le r \le r_3)$ and surrounding rock $(r_3 \le r \le R)$ are obtained as follows, respectively:

$$h_{slw} = H_w \cdot \frac{k_2 k_3 k_4 \ln \frac{r_1}{r_0} \ln \frac{r}{r_0}}{(a+b) \ln \frac{r_1}{r_0}} \left(r_0 \le r \le r_1 \right) \tag{10}$$

$$h_{flw} = H_w \cdot \frac{b \ln \frac{r}{r_1} + k_2 k_3 k_4 \ln \frac{r_1}{r_0} \ln \frac{r_2}{r}}{(a+b) \ln \frac{r_2}{r_1}} \left(r_1 \le r \le r_2 \right) \tag{11}$$

$$h_{gw} = H_w \cdot \frac{b \ln \frac{r_3}{r_2} + k_1 k_2 k_4 \ln \frac{r_3}{r_2} \ln \frac{r}{r_2}}{(a+b) \ln \frac{r_3}{r_2}} \left(r_2 \le r \le r_3 \right) \tag{12}$$

$$h_{rw} = H_w \cdot \frac{a \ln \frac{r}{r_3} + b \ln \frac{R}{r_3} + k_1 k_2 k_4 \ln \frac{r_3}{r_2} \ln \frac{R}{r}}{(a+b) \ln \frac{R}{r_3}} \left(r_3 \le r \le R \right), \tag{13}$$

where the coefficients a and b are determined by Eqs. (14) and (15):

$$a = k_1 k_2 k_3 \ln \frac{R}{r_3} + k_1 k_2 k_4 \ln \frac{r_3}{r_2} \tag{14}$$

$$b = k_2 k_3 k_4 \ln \frac{r_1}{r_0} + k_1 k_3 k_4 \ln \frac{r_2}{r_1}. \tag{15}$$

The relationship between the tunnel discharge Q and the hydraulic head h at each position of the tunnel is displayed as

$$Q = kA(r) \frac{dh}{dr}, \tag{16}$$

where $A(r)$ is the cross-sectional area of the seepage.

Consequently, combining Eqs. (10–13) with (16), the tunnel discharge at each position can be solved with the far-field radius R and the far-field head H_w obtained by related geological reports. Moreover, the tunnel discharge per unit length Q_w under the influence of the far-field water head after the tunnel completed can be resulted into

$$Q_w = \frac{2\pi k_1 k_2 k_3 k_4}{a+b} H_w \tag{17}$$

Water discharge induced by water-bearing fault head

(1) Water discharge in surrounding rock.

This paper introduces the complex variable method to obtain the magnitude of the water discharge in the surrounding rock, as illustrated in Fig. 3. The physical domain is separated into two parts: the inside and the outside of the tunnel. In the z-plane:

$$z = x + iy. \tag{18}$$

Through conformal mapping, the boundary curves outside the grouting ring L_3 and the fault boundary $A - A'$ in z-plane are mapped into two concentric circular curves Γ_1 and Γ_2 in ζ-plane, respectively. The radius of Γ_1 and Γ_2 are α and 1. The surrounding rock zone outside the grouting ring and the fault boundary in z-plane is mapped into the concentric ring area in ζ-plane. In the ζ-plane

$$\zeta = \varepsilon + i\eta. \tag{19}$$

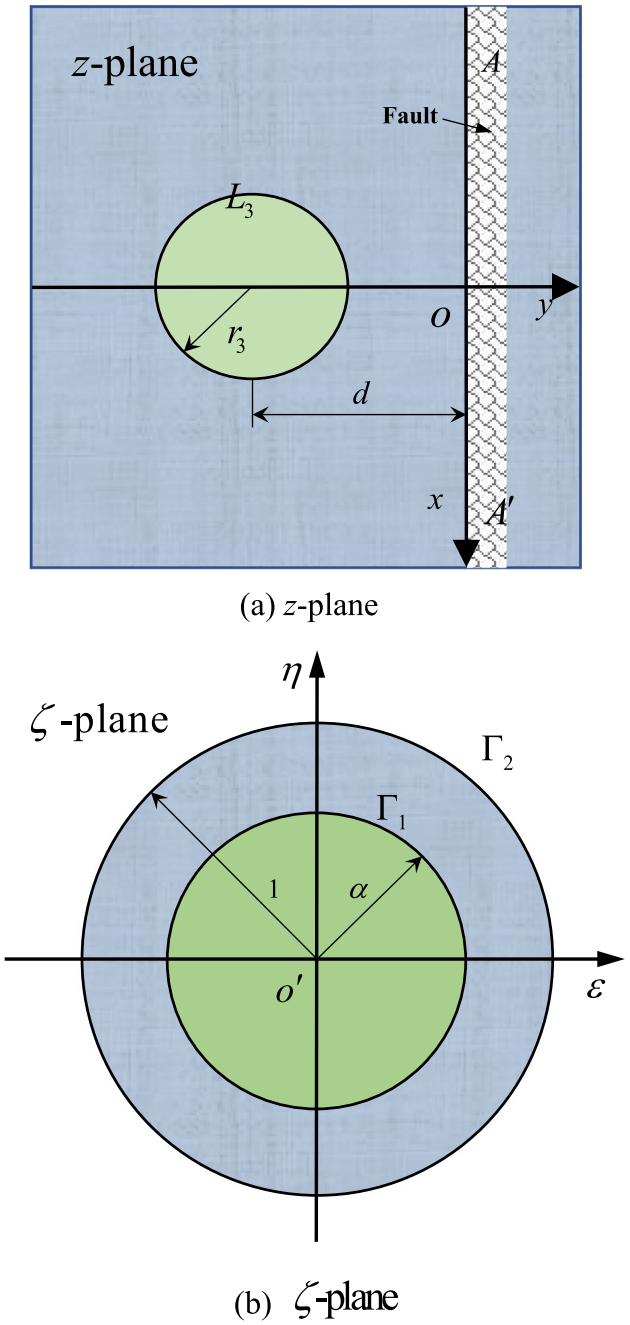

Fig. 3 Conformal mapping type. (**a**) z-plane. (**b**) ζ - plane

The mapping formula is as follows:

$$z = \omega(\zeta) = -id\frac{1-\alpha^2}{1+\alpha^2}\cdot\frac{1+\zeta}{1-\zeta}, \tag{20}$$

in which d is the distance between the tunnel centerline and water-bearing fault $A-A'$, and $\omega(\zeta)$ is an analytical function in ζ-plane. The coefficient α can be obtained from Eq. (21):

$$\frac{r}{d} = \frac{2\alpha}{1+\alpha^2}, \tag{21}$$

where the α values between zero and one.

In the circular area of ζ-plane, supposing the density of groundwater is constant, the discharge per unit length through the circular tunnel with the radius ρ can be expressed as

$$Q = 2\pi\rho|V|, \tag{22}$$

where V is the velocity of the radial seepage, and $|V|$ is defined as

$$|V| = -\frac{\partial\varphi}{\partial\rho}, \tag{23}$$

in which φ is the potential function.

Substituting Eq. (23) into Eq. (22), it results into

$$\frac{Q}{2\pi\rho} = -\frac{\partial\varphi}{\partial\rho}. \tag{24}$$

Integrating about Eq. (24), the head H at radius ρ is obtained as follows:

$$H = -\frac{\varphi}{k} = \frac{Q}{2\pi k}\ln\rho + m, \tag{25}$$

where the constant m is determined by the corresponding boundary conditions.

At the fault boundary $A-A'(|\zeta|=1)$, the hydraulic head is $H = H_f$, as embodied in Fig. 1b. Substituting the fault boundary condition into Eq. (25), it can be derived as

$$m = H_f. \tag{26}$$

The head at the boundary between the grouting ring and the surrounding rock L_3 is assumed as h_3', the water discharge through the interface can be written as

$$Q = \frac{2\pi k_4\left(h_3' - H_f\right)}{\ln\alpha}. \tag{27}$$

(2) Water discharge in the grouting ring and lining

As noted in Fig. 2, the secondary lining, primary lining and grouting ring are annular zones with $r_0 \le r \le r_1$, $r_1 \le r \le r_2$, $r_2 \le r \le r_3$, respectively. Similarly, the water head at L_1, L_2 and L_3 induced by the fault are assumed as h_1', h_2' and h_3', respectively.

On the basis of Eqs. (2) and (8), the expressions of the head in the lining on account of effect on the fault head h_3' can be expressed as follows:

$$h' = \begin{cases} \dfrac{k_2 \ln \frac{r}{r_0}}{a' + b'} \cdot h_3' \left(r_0 \le r \le r_1\right) \\ \dfrac{k_2 \ln \frac{r_1}{r_0} \ln \frac{r_2}{r} + b' \ln \frac{r}{r_1}}{(a' + b') \ln \frac{r_2}{r_1}} \cdot h_3' \left(r_1 \le r \le r_2\right) \\ \dfrac{a' \ln \frac{r}{r_2} + b' \ln \frac{r_3}{r_2}}{(a' + b') \ln \frac{r_3}{r_2}} \cdot h_3' \left(r_2 \le r \le r_3\right) \end{cases}, \tag{28}$$

where $a' = \frac{k_1 k_2}{k_3} \ln \frac{r_3}{r_2}$, and $b' = k_1 \ln \frac{r_2}{r_1} + k_2 \ln \frac{r_1}{r_0}$.

The water discharge at the interface between the grouting ring and surrounding rock L_3 expressed by h_3' is written as follows:

$$Q = \frac{2\pi k_3 a'}{(a' + b') \ln \frac{r_3}{r_2}} \cdot h_3'. \tag{29}$$

Combining Eq. (27) with Eq. (29), it leads to

$$h_3' = H_f \cdot \frac{k_4 \left(a' + b'\right) \ln \frac{r_3}{r_2}}{k_4 (a' + b') \ln \frac{r_3}{r_2} - k_3 a' \ln \alpha}. \tag{30}$$

Then, by combining Eqs. (16), (28) with Eq. (30), it results that the water discharge of the tunnel under the water-bearing fault head is obtained as

$$Q_f = \frac{2\pi k_1 k_2}{a' + b'} \cdot h_3' = \frac{2\pi k_1 k_2 k_4 H_f}{k_4 (a' + b') \ln \frac{r_3}{r_2} - k_3 a' \ln \alpha}. \tag{31}$$

Consequently, the magnitude of the tunnel discharge is attained by superposing the far-field head and the fault head, not taking the coupling effect of seepage field into account. The total discharge of tunnel Q in high head region and that adjacent to fault can be written into the following form:

$$Q = Q_w + Q_f = \frac{2\pi k_1 k_2 k_3 k_4}{a + b} H_w + \frac{2\pi k_1 k_2 k_4 H_f}{k_4 (a' + b') \ln \frac{r_3}{r_2} - k_3 a' \ln \alpha}, \tag{32}$$

in which Q_w and Q_f are the tunnel discharge induced by the far-field head and water-bearing fault head, respectively.

Solution of seepage field in surrounding rock of tunnel adjacent to water-bearing fault

Analytical model for virtual image method

This paper introduces the virtual image method to obtain the solution of the seepage field for tunnel surrounding rock adjacent to the water-bearing fault. For a tunnel near the fault, it is reasonably assumed that the tunnel is a pumping well in an infinite area, then it can be obtained the injection well by means of mirroring on the other side of the fault. The solution can be derived by taking the superimposed effect of the pumping well and an image injection well into account to investigate the potential of any observation point in surrounding rock region, as shown in Fig. 4.

The seepage potential function of a single well in an infinite area is expressed as

$$\Phi = \frac{Q}{2\pi} \ln \rho + C, \tag{33}$$

where Φ is the seepage potential function; ρ is the distance from the observation point at the surrounding rock to the pumping well centerline; Q is the flow rate of the pumping well; C is a constant determined by the related boundary conditions.

The pumping well and the image injection well have the same flow rate, as performed in Fig. 4. Therefore, the potential function of the pumping well and injection well are assumed as Φ_1 and Φ_2, respectively. They can be written as

$$\Phi_1 = \frac{Q}{2\pi} \ln \rho_1 + C_1 \tag{34}$$

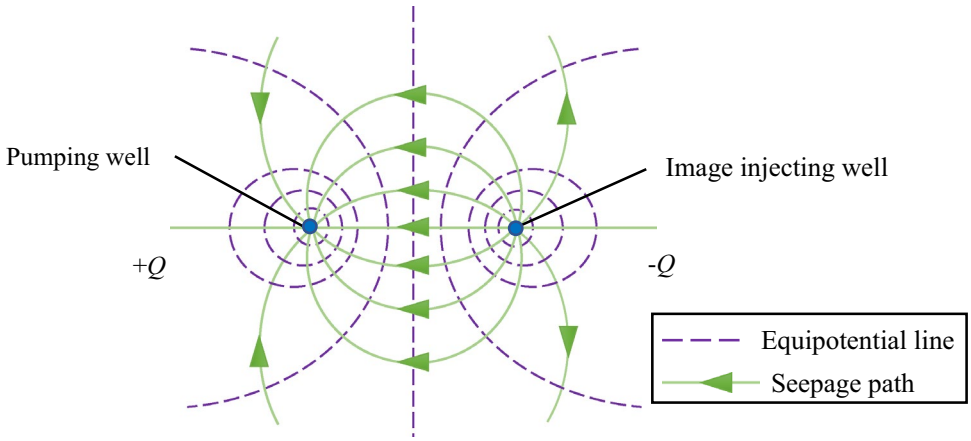

Fig. 4 Model of well flow theory

$$\Phi_2 = \frac{-Q}{2\pi} \ln \rho_2 + C_2, \tag{35}$$

in which ρ_1 and ρ_2 are the distance from the observation point to the pumping well and the injection well, respectively.

According to the superposition principle of potential, the expression of the potential function in surrounding rock can be written as

$$\Phi = \Phi_1 + \Phi_2 = \frac{Q}{2\pi} \ln \rho_1 - \frac{Q}{2\pi} \ln \rho_2 + C_1 + C_2 = \frac{Q}{2\pi} \ln \frac{\rho_1}{\rho_2} + C. \tag{36}$$

The potential $\Phi = C$ at the position $\rho_1 = \rho_2$(the central line of two wells) due to the interaction between the pumping well and the injection well, which indicates an equipotential line at the central line. Consequently, the line can be regarded as a water supply boundary with a constant hydraulic head, which is in line with the geological conditions of a continuous water supply fault herein. Therefore, the seepage of the geological conditions of the fault adjacent tunnel which is filled with water continuously can be analyzed by the model in this work.

Solution of potential function of seepage field

The geological conditions with faults on the side are simplified to obtain the seepage mechanics model, as plotted in Fig. 5. The rectangular coordinate system is established with the tunnel center as the origin, the vertical direction as the y axis and the horizontal direction as the x axis, respectively. The tunnel structure is divided into three parts: the primary lining, secondary lining and grouting ring from inside to outside. The distance between the center of the left circular tunnel and the boundary $A - A'$ of the fault zone is defined as d; the coordinate of the center of the tunnel image is $O'(2d, 0)$. The flow of both the solid tunnel and the image tunnel are denoted by Q, and the head at the fault boundary $(y = d)$ is H_f. Consequently, according to the principle of the virtual image method and the superposition method, the potential function of arbitrary observation point $P(x, y)$ on the surrounding rock in an infinite area can be expressed as

$$\Phi = \frac{Q}{2\pi} \ln \frac{\rho_1}{\rho_2} + \Phi_c = \frac{Q}{2\pi} \ln \frac{\sqrt{x^2 + y^2}}{\sqrt{(x - 2d)^2 + y^2}} + \Phi_c \tag{37}$$

$$\Phi = \frac{Q}{2\pi} \ln \frac{\rho_1}{\rho_2} + \Phi_c = \frac{Q}{2\pi} \ln \frac{\sqrt{x^2 + y^2}}{\sqrt{x^2 + y^2 + 4d(d - x\cos\beta - y\sin\beta)}} + \Phi_c. \tag{38}$$

Furthermore, Eqs. (37) and (38) can be written into polar coordinates as follows:

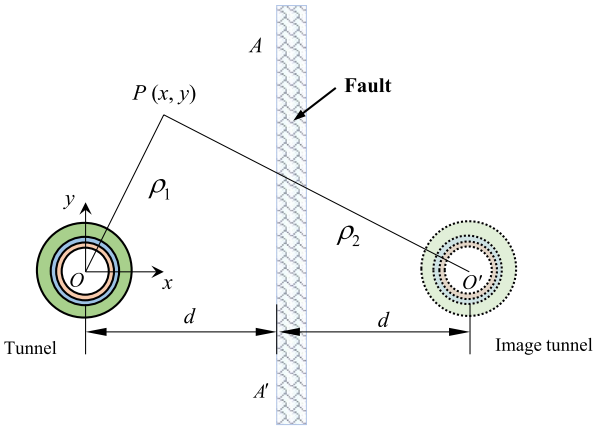

(a) Vertical fault

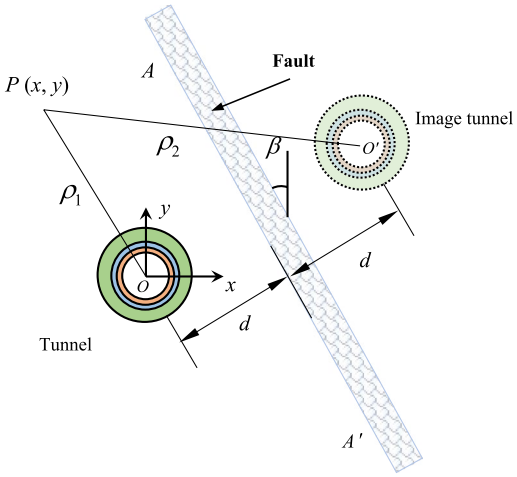

(b) Inclined fault

Fig. 5 Schematic diagram of virtual image method considering fault dip angle. (**a**) Vertical fault. (**b**) Inclined fault

$$\Phi = \frac{Q}{2\pi} \ln \frac{r}{\sqrt{r^2 - 4dr\cos\theta + 4d^2}} + \Phi_c \tag{39}$$

$$\Phi = \frac{Q}{2\pi} \ln \frac{r}{\sqrt{r^2 + 4d^2 - 4dr\cos(\theta - \beta)}} + \Phi_c, \tag{40}$$

where Eqs. (37) and (39) are related to the vertical fault, while Eqs. (38) and (40) are related to the inclined fault with a dip of β. ρ_1 and ρ_2 are the distances from the observation point at the surrounding rock or the lining to the center of tunnel and the image tunnel, respectively. Φ_c is the potential

at the fault boundary ($x = d$), $\Phi_c = \frac{1}{2}\overline{k}H_f^2$, in which $\overline{k}$ is the equivalent permeability coefficient ($\overline{k} = \int_{r_0}^{r} k\mathrm{d}r$), that is, the mean magnitude of the permeability coefficient from r_0 to the water head position r.

Correction of potential function in seepage field

Compared with the surrounding rock, the tunnel cavity is relatively small so that the potential functions around the tunnel are obtained as Eqs. (37–40) based on the well flow theory of the virtual image method. The tunnel and the mapped image tunnel are regarded as a pumping well and an injection well, regardless of the circular cavity excavated. However, the tunnel discharges water in a certain range in the authentic construction, which manifests Eqs. (37–40) are only applicable to far surrounding rock. The error of the potential function approaches to a larger value as the testing point is closer to the tunnel. For example, the actual value of the potential at the boundary curve of the secondary lining L_0 is 0, but according to Eq. (39), the potential is

$$\Phi = \frac{Q}{2\pi}\ln\frac{r_0}{\sqrt{r_0^2 - 4dr_0\cos\theta + 4d^2}} + \Phi_c \neq 0, \tag{41}$$

which is clearly not in line with the actual situation. Therefore, it is necessary to modify the seepage function around the tunnel for higher accuracy. Therefore, this paper refers to Kim and Eisenstein (2006) for the correction of the pressure on the lining to propose a correction method as follows.

Supposing $\overline{\Phi}$ represents the potential after correction, the potential at $r = r_0$ and $r = \infty$ can be written as

$$\begin{cases} \overline{\Phi}\big|_{r=r_0} = 0 \\ \overline{\Phi}\big|_{r=\infty} = \Phi|_{r=\infty} \end{cases}. \tag{42}$$

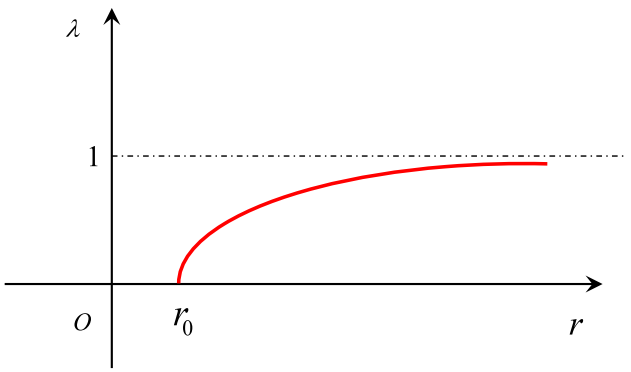

Fig. 6 Corrected function characteristic curve

In this paper, a modified function $\lambda = f(r)$ is introduced, and the variable r varies from $(r_0, +\infty)$. The characteristic curve of $\lambda = f(r)$ is shown in Fig. 6.

According to the characteristic curve, a more reasonable correction function is proposed as

$$\lambda = f(r) = 1 - \frac{r_0}{r}. \tag{43}$$

Concerned on the vertical fault, the corrected potential function in rectangular and polar coordinates can be written as

$$\overline{\Phi} = \left(1 - \frac{r_0}{r}\right)\left(\frac{Q}{2\pi}\ln\frac{\sqrt{x^2+y^2}}{\sqrt{(x-2d)^2+y^2}} + \Phi_c\right), \tag{44}$$

$$\overline{\Phi} = \left(1 - \frac{r_0}{r}\right)\left(\frac{Q}{2\pi}\ln\frac{r}{\sqrt{r^2 - 4dr\cos\theta + 4d^2}} + \Phi_c\right). \tag{45}$$

In addition, the functions considering the inclined fault are listed below:

$$\overline{\Phi} = \left(1 - \frac{r_0}{r}\right)\frac{Q}{2\pi}\ln\frac{\sqrt{x^2+y^2}}{\sqrt{x^2+y^2+4d(d - x\cos\beta - y\sin\beta)}} + \Phi_c \tag{46}$$

$$\overline{\Phi} = \left(1 - \frac{r_0}{r}\right)\frac{Q}{2\pi}\ln\frac{r}{\sqrt{r^2 + 4d^2 - 4dr\cos(\theta - \beta)}} + \Phi_c. \tag{47}$$

Solution of head in tunnel structure and seepage field of surrounding rock

Considering the tunnel is in the phreatic aquifer, it is indispensable to investigate the head distribution in the tunnel structure and surrounding rock. In the phreatic aquifer, the potential function $\overline{\Phi}$ is (Girinskii 1946; Bear 1972; Chen et al. 2006):

$$\overline{\Phi} = \int_0^h khdh + C_u = \frac{1}{2}kh^2 + c_u, \tag{48}$$

where h is the total hydraulic head, and C_u is a constant usually taken as 0.

(1) The potential function $\overline{\Phi}_{sl}$ in the secondary lining area $(r_0 \le r \le r_1)$ can be written as

$$\overline{\Phi}_{sl} = \int_0^h k_1 h\mathrm{d}h. \tag{49}$$

Consequently, the head of the second lining area h_{sl} can be expressed as

$$h_{sl} = \sqrt{\frac{2\overline{\Phi}_{sl}}{k_1}} = \sqrt{\frac{2\left(1-\frac{r_0}{r}\right)\left(\frac{Q}{2\pi}\ln\frac{r_1}{r_2}+\Phi_c\right)}{k_1}}. \tag{50}$$

Thus, the head h_1 on curve L_1 for the vertical fault can be derived as

$$h_1 = \left[\frac{Q\left(1-\frac{r_0}{r_1}\right)}{\pi k_1}\ln\frac{r_1}{\sqrt{r_1^2-4r_1 d\cos\theta+4d^2}}+\frac{\left(1-\frac{r_0}{r_1}\right)k_1H_f^2}{k_1}\right]^{\frac{1}{2}}, \tag{51}$$

while the head h_1 on curve L_1 for the inclined fault is

$$h_1 = \left[\frac{Q\left(1-\frac{r_0}{r_1}\right)}{\pi k_1}\ln\frac{r}{\sqrt{r^2+4d^2-4dr\cos(\theta-\beta)}}+\frac{\left(1-\frac{r_0}{r_1}\right)k_1H_f^2}{k_1}\right]^{\frac{1}{2}}. \tag{52}$$

(2) In the primary lining area $\left(r_1 \le r \le r_2\right)$, the potential function $\overline{\Phi}_{fl}$ is written from Eq. (44) as

$$\overline{\Phi}_{fl} = \int_0^{h_1} k_1 h\mathrm{d}h + \int_{h_1}^{h_2} k_2 h\mathrm{d}h = \overline{\Phi}_1 + k_1h_1\left(h-h_1\right)+\frac{1}{2}k_2\left(h-h_1\right)^2, \tag{53}$$

where $\overline{\Phi}_1$ denotes the potential at the interface curve L_1 between the secondary lining and the primary lining, and it can be obtained by Eqs. (54) and (55) as

$$\overline{\Phi}_1 = \left(1-\frac{r_0}{r_1}\right)\left(\frac{Q}{2\pi}\ln\frac{r_1}{\sqrt{r_1^2-4dr_1\cos\theta+4d^2}}+\Phi_c\right) \tag{54}$$

$$\overline{\Phi}_1 = \left(1-\frac{r_0}{r_1}\right)\left(\frac{Q}{2\pi}\ln\frac{r_1}{\sqrt{r_1^2+4d^2-4dr_1\cos(\theta-\beta)}}+\Phi_c\right), \tag{55}$$

in which Eqs. (54) and (55) are for the vertical fault and the inclined fault derived by Eqs. (45) and (47), respectively.

Thus, the head of the primary lining area h_{fl} can be solved by Eq. (53) as

$$\begin{aligned} h_{fl} =& h_1 - \frac{k_1}{k_2}h_1 + \frac{1}{k_2}\Big[\left(k_2h_1-k_1h_1\right)^2 \\ & -2k_2\left(\frac{1}{2}k_2h_1^2-k_1h_1^2-\overline{\Phi}_{fl}+\overline{\Phi}_1\right)\Big]^{\frac{1}{2}} \\ =& h_1-\frac{k_1}{k_2}h_1+\sqrt{\frac{k_1^2}{k_2^2}h_1^2+\frac{2}{k_2}\left(\overline{\Phi}_{\mathrm{fl}}-\overline{\Phi}_1\right)}. \end{aligned} \tag{56}$$

The head h_2 on curve L_2 can be attained as

$$h_2 = h_1 - \frac{k_1}{k_2}h_1 + \sqrt{\frac{k_1^2}{k_2^2}h_1^2+\frac{2}{k_2}\left(\overline{\Phi}_2-\overline{\Phi}_1\right)}, \tag{57}$$

where

$$\overline{\Phi}_2 = \left(1-\frac{r_0}{r_2}\right)\left(\frac{Q}{2\pi}\ln\frac{r_2}{\sqrt{r_2^2-4dr_2\cos\theta+4d^2}}+\Phi_c\right) \tag{58}$$

or

$$\overline{\Phi}_2 = \left(1-\frac{r_0}{r_2}\right)\left(\frac{Q}{2\pi}\ln\frac{r_2}{\sqrt{r_2^2+4d^2-4dr_2\cos(\theta-\beta)}}+\Phi_c\right), \tag{59}$$

in which Eqs. (58) and (59) are for the vertical fault and the inclined fault, respectively.

(3) In the grouting ring area ($r_2 \le r \le r_3$), the potential function $\overline{\Phi}_g$ is written as follows:

$$\begin{aligned} \overline{\Phi}_g =& \int_0^{h_1} k_1 h\mathrm{d}h + \int_{h_1}^{h_2} k_2 h\mathrm{d}h + \int_{h_2}^{h} k_3 h\mathrm{d}h \\ =& \overline{\Phi}_2 + \left[k_1h_1+k_2\left(h_2-h_1\right)\right]\cdot\left(h-h_2\right)+\frac{1}{2}k_3\left(h-h_2\right)^2. \end{aligned} \tag{60}$$

Thus, the head of the grouting ring area h_g can be solved by Eq. (60) as

$$\begin{aligned} h_g =& h_2+\frac{1}{k_3}\Big\{\left(k_2-k_1\right)h_1-k_2h_2+\Big[\left(k_1h_1\right. \\ & \left.+\ k_2h_2-k_2h_1\right)^2-2k_3\left(\overline{\Phi}_2-\overline{\Phi}_g\right)\Big]^{\frac{1}{2}}\Big\}. \end{aligned} \tag{61}$$

The head h_3 on curve L_3 can be derived as

$$\begin{aligned} h_3 =& h_2+\frac{1}{k_3}\Big\{\left(k_2-k_1\right)h_1-k_2h_2+\Big[\left(k_1h_1\right. \\ & \left.+\ k_2h_2-k_2h_1\right)^2-2k_3\left(\overline{\Phi}_2-\overline{\Phi}_3\right)\Big]^{\frac{1}{2}}\Big\}, \end{aligned} \tag{62}$$

where

$$\overline{\Phi}_3 = \left(1-\frac{r_0}{r_3}\right)\left(\frac{Q}{2\pi}\ln\frac{r_3}{\sqrt{r_3^2-4dr_3\cos\theta+4d^2}}+\Phi_c\right) \tag{63}$$

or

$$\overline{\Phi}_3 = \left(1 - \frac{r_0}{r_3}\right)\left(\frac{Q}{2\pi}\ln\frac{r_3}{\sqrt{r_3^2 + 4d^2 - 4dr_3\cos(\theta - \beta)}} + \Phi_c\right), \tag{64}$$

in which Eqs. (63) and (64) are for the vertical fault and the inclined fault, respectively.

(4) Likewise, the potential function of the surrounding rock ($r \geq r_3$) can be derived as

$$\overline{\Phi_r} = \int_0^{h_1} k_1 h\mathrm{d}h + \int_{h_1}^{h_2} k_2 h\mathrm{d}h + \int_{h_2}^{h_3} k_3 h\mathrm{d}h + \int_{h_3}^{h_4} k_4 h\mathrm{d}h. \tag{65}$$

Thus, the head of the surrounding rock h_r can be attained as

$$h_r = h_3 + \frac{1}{k_4}\left\{\left(k_2h_1 + k_3h_2 - k_1h_1 - k_2h_2 - k_3h_3\right) + \left[\left(k_2h_1 + k_3h_2 - k_1h_1 - k_2h_2 - k_3h_3\right)^2 - 2k_4\left(\overline{\Phi}_3 - \overline{\Phi}_r\right)\right]^{\frac{1}{2}}\right\}. \tag{66}$$

Consequently, the distribution of seepage field in the structure and surrounding rock of the tunnel in the phreatic aquifer can be obtained from Eqs. (50), (56), (61) and (66).

Superposing the seepage field and gravity field, the pressure head is written as

$$h_p = h - y, \tag{67}$$

where h sums up the hydraulic head of the secondary lining, primary lining, grouting ring and surrounding rock, and y is the vertical coordinate of the observation point.

In sum, the seepage field at arbitrary points in the surrounding rock around the circular deep tunnel and the distribution of the total head on the tunnel structure are finally derived by employing the virtual image method and the seepage theory, considering the effects of the water-bearing fault in the water-rich mountain region.

Case verification

Very limited engineering project data were publicly available for head on tunnel structure due to the influence of water-bearing fault. In this paper, the degenerated analytical solutions are compared with the existing ones, while the numerical results established based on the geological condition of the deep buried tunnel are compared to examine the accuracy and reliability of the presented analytical solutions.

Comparison with Harr analytical solution

The seepage of tunnel is derived in this paper, considering the effects of the grouting ring and the lining. Meanwhile, the solutions could be degenerated to compare with the hydraulic Harr solutions (Harr 1962), not taking the influence of the grouting ring and the tunnel lining into account. The value of permeability coefficient is considered as the same as that of surrounding rock. The water-bearing fault in this study is equivalent to the groundwater level in the Harr solution (Harr 1962), which is regarded as the water-bearing source line, leaving out the influence of far-field head. Figure 7 plots the seepage field of surrounding rock considering the water-bearing fault on the left side of the tunnel. The pressure hydraulic head on some concerned locations are compared between the analytical solution in this paper and the Harr solution to have insight into the distribution of seepage field. The results are exhibited in Fig. 8, where lines AB, CD, JF and DE are in the vertical direction, while lines BI and GH are in the horizontal direction.

Good agreements are shown in Figs. 7 and 8 on between the Harr solution (Harr 1962) and the degenerated analytic solution in this paper on the seepage field of the surrounding rock of deep buried tunnel, considering the influence of water-bearing fault. In the vertical centerline of tunnel (lines AB and JF), the pressure head increases and then decreases between the water source line and the tunnel due to the constant water supply above the tunnel cavity. The pressure head increases in steady under the tunnel centerline. The pressure hydraulic head on the tunnel sideline (lines CD and DE) is consistent with the trend of the head in the vertical tunnel centerline, while the pressure head on the sideline is

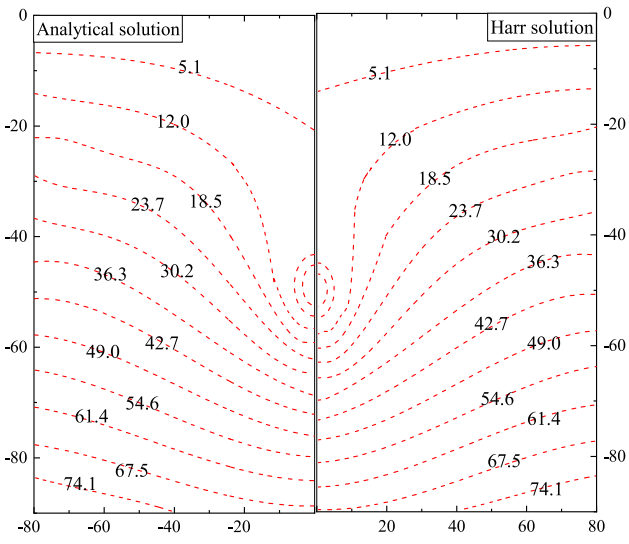

Fig. 7 Comparison of seepage field between analytical solution and Harr solution

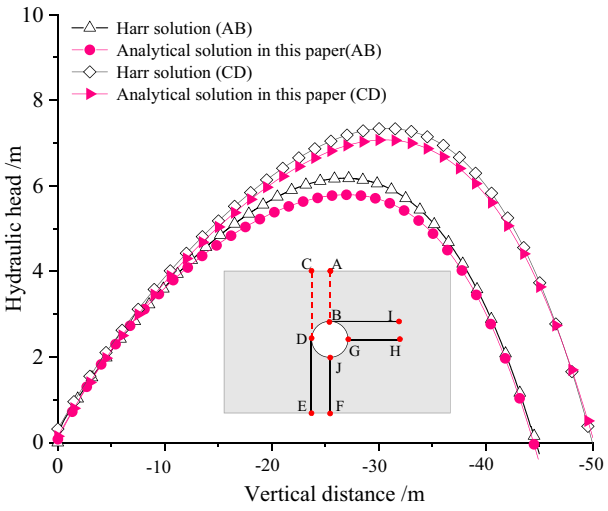

(a) Line AB and CD

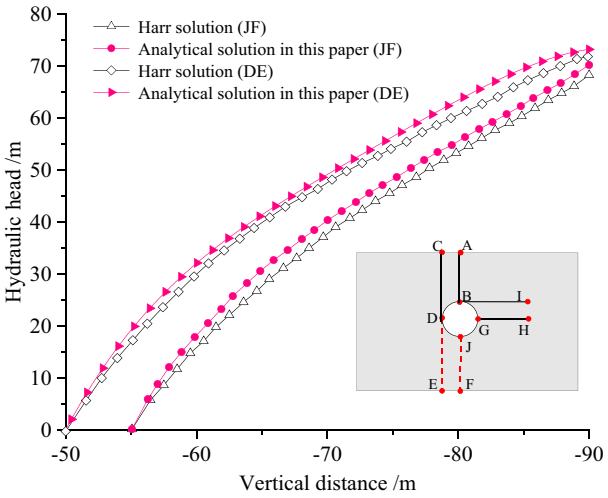

(b) Line JF and DE

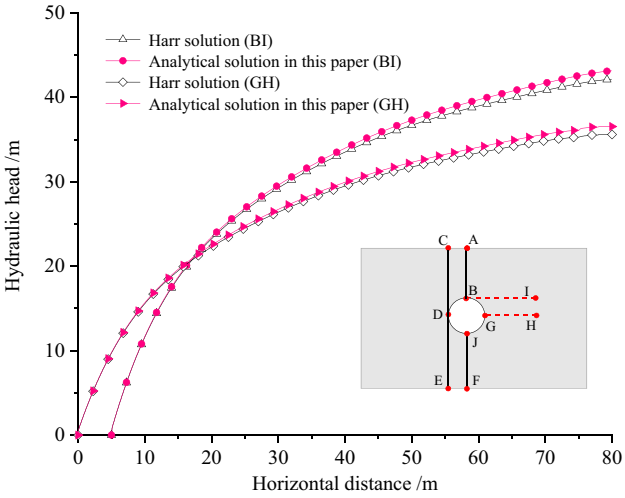

(C) Line BI and GH

Fig. 8 Comparison of pressure head of surrounding rock. (**a**) Line AB and CD, (**b**) Line JF and DE, (**c**) Line BI and GH

larger in the same level. The seepage field on the both sides of the tunnel is symmetrically distributed in the horizontal direction (lines BI and GH). Moreover, the pressure head increases rapidly around the cavity, while the rate of head growth gradually levels off far away from the tunnel.

In summary, it indicates that the degenerated analytical solution proposed in this paper has a relative accuracy on seepage filed of surrounding rock. In addition, the Harr solution (Harr 1962) could be used to solve the seepage field of surrounding rock below the groundwater level, no considering the influence of lining and grouting ring. Consequently, the analytical solution in this paper will be more accurate when taking the effect of fault, lining and grouting ring into account.

Comparison with numerical simulation solution

The numerical model is established based on the deep buried Niuheling tunnel in China to investigate the seepage filed, as demonstrated in Fig. 9. The Niuheling tunnel is planned to be built in Lishui, Zhejiang Province. The tunnel undergoes a great deal of low hills with large topographic relief and V-shaped gullies developed. The altitude varies from 235 m to 522.4 m, and the relative height difference is from 10 m to 287.4 m with a slope from 25° to 60°. The stratum lithology is mainly the siltstone and tuff of the upper Cretaceous formation. Large amount of water stays in gullies all the year round, and the level in the reservoir are greatly affected by the seasons. What's more, there are many faults in the deep buried section, and most of the faults are filled with water, supplied from the reservoir or valley.

Based upon the existing practical engineering, the model sets 100 m both in height and width. The radius of tunnel is 5 m, and the head sets up zero at the cavity. The distance from the edge of the fault to the tunnel centerline d is 20 m. The tunnel model is separated into three parts from inside to outside: the secondary lining, primary lining and grouting ring, and the corresponding permeability coefficients and thicknesses are indicated in Table 2. To facilitate the calculation and comparison with the analytical solution, this paper simplifies the numerical model and sets the thickness of secondary lining and primary lining as 0.5 m. In this model, the natural head of water-bearing fault is 100 m. The tunnel center and the level of the groundwater are 105 m and 5 m below the surface, respectively. The far field stable head can be expressed by the original head of the tunnel centerline before the tunnel excavation without considering the groundwater flow. In the simulation, the far-field stable pressure head is adopted as 55 m. Based on the actual projects and Bobet (2003), the magnitude of far-field radius is

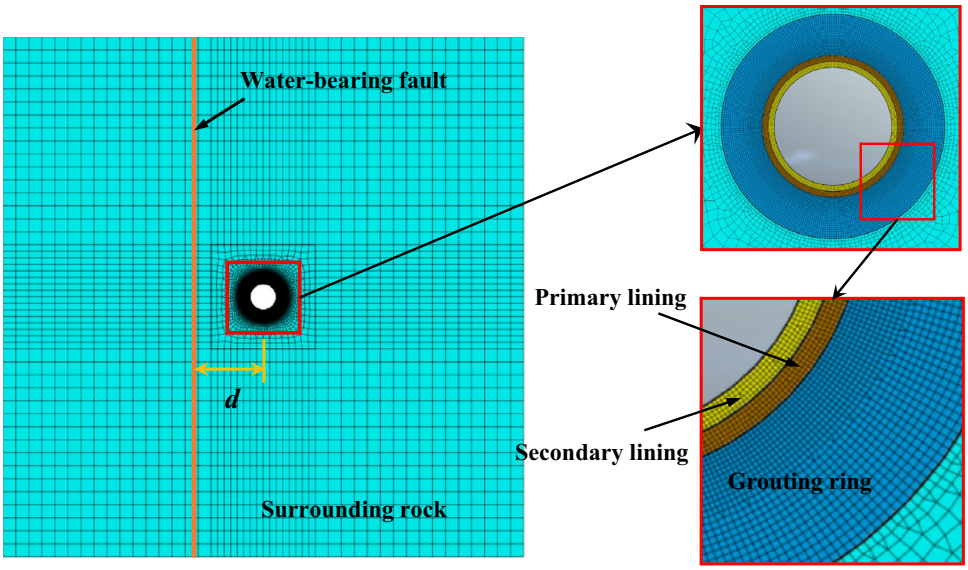

Fig. 9 Mesh modelling in finite element simulation method

Table 2 Related tunnel parameters

	Permeability coefficient (m/s)	Thickness (m)
Secondary lining	2×10^{-10}	0.5
Primary lining	4×10^{-10}	0.5
Grouting circle	2×10^{-8}	3.5
Surrounding rock	6×10^{-6}	/

approximately 6–10 times of the tunnel radius, while the far-field radius is set as 45 m in this numerical model.

According to the simplified assumptions above, it is presumed that the surrounding rock is an isotropic homogeneous continuous medium, and the groundwater is incompressible and conforms to the law of the stable seepage in the numerical model. The grid size of the surrounding rock is taken as 2.5 m or 5 m, and it sets 0.1 m at the lining and grouting ring. The model has a total of 15,493 nodes and 15,419 elements after discretization.

In this paper, the contour map of the seepage field on the right side of the fault is extracted and plotted compared with the analytical solution, as demonstrated in Fig. 10. It can be derived from Fig. 10 that the distribution of the seepage field of the surrounding rock under the influence of water-bearing fault obtained by the numerical simulation and theoretical analysis is in good agreement with the shape and trend of its equal hydraulic head line. What's more, the analytical solution is better fitted with numerical solution at the region closer to the tunnel cavity.

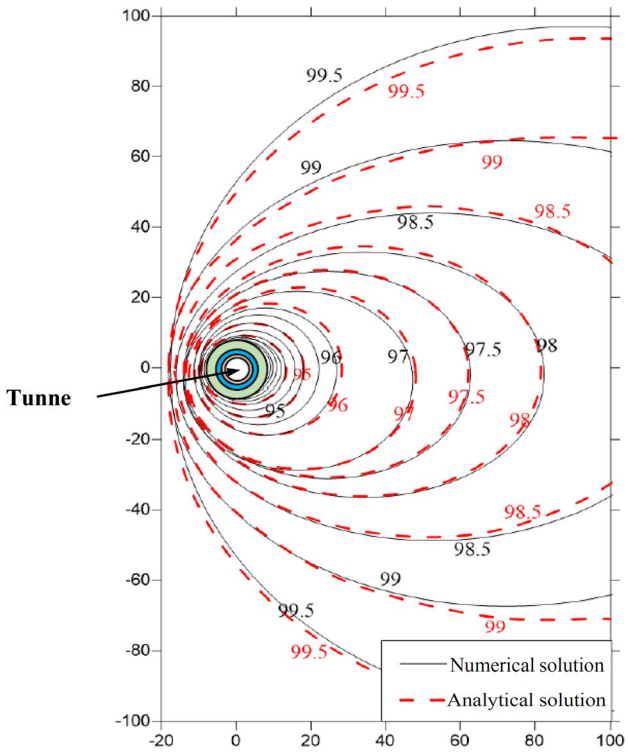

Fig. 10 Water head line diagram on right side of fault

It is observed that the contour lines of the hydraulic head are very dense on the tunnel structure and too small compared with the head on the surrounding rock in Fig. 10. Consequently, this paper adopts the data contrast to verify the accuracy of the theoretical solution of the hydraulic

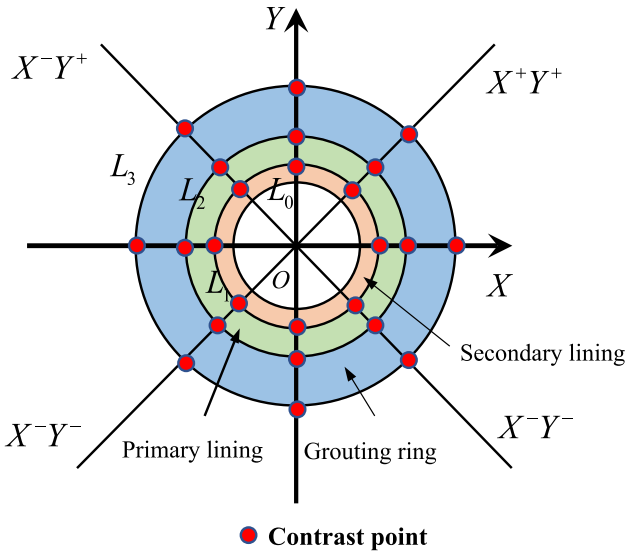

Fig. 11 Schematic diagram of contrast point position

head on the tunnel structure in the hope that it can better reflect the influence of the head on the hydraulic head of the tunnel structure. This work establishes the rectangular coordinate system, which takes the coordinate center as the origin, the horizontal and vertical direction as *X*-axis and *Y*-axis, respectively. The numerical and analytical solutions of the hydraulic head are compared on the intersection of *X*-axis, *Y*-axis and quadrant bisector with tunnel structure L_1, L_2 and L_3 under the case of different heads of the water-bearing fault. The locations of the contrast points are plotted in Fig. 11.

X^+Y^+ represents the bisector of the first quadrant as well as the other quadrants. The comparison results between the numerical solution and analytical solution of hydraulic head on tunnel structure are exhibited in Tables 3, 4, 5. The relative error is the ratio of the difference between the numerical results and the analytical results.

Combining Fig. 10 and Tables 3, 4, 5, it can be concluded that the seepage field obtained by the theoretical method in this paper is relatively consistent with the seepage field acquired by the numerical simulation, which indicates the value of hydraulic head on the tunnel structure is nearly identical. However, it can be observed from the comparison with the data listed in Tables 3, 4, 5 that the numerical results are larger in the Y^- direction below the tunnel. Meanwhile, the results of the numerical simulation are smaller

Table 3 Comparison of numerical solution and analytical solution of water head on tunnel structure (H_f = 100 m)

	L_1			L_2			L_3		
	Analytical solution	Numerical solution	Relative error	Analytical solution	Numerical solution	Relative error	Analytical solution	Numerical solution	Relative error
X^+	20.34 m	20.51 m	−0.8%	30.25 m	30.89 m	−2.1%	90.38 m	91.66 m	−1.4%
X^+Y^+	20.54 m	20.21 m	1.6%	30.44 m	29.62 m	2.7%	90.47 m	88.77 m	1.8%
Y^+	20.71 m	19.53 m	4.8%	30.71 m	29.03 m	5.5%	90.85 m	89.01 m	2.0%
X^-Y^+	21.66 m	20.76 m	4.2%	31.54 m	30.26 m	4.1%	91.63 m	89.42 m	2.4%
X^-	22.12 m	21.87 m	1.1%	32.26 m	33.05 m	−2.4%	92.41 m	93.60 m	−1.3%
X^-Y^-	21.66 m	22.47 m	−3.7%	31.54 m	32.67 m	−3.6%	91.63 m	93.17 m	−1.7%
Y^-	20.71 m	21.34 m	−3.0%	30.71 m	32.09 m	−4.5%	90.85 m	93.47 m	−2.9%
X^+Y^-	20.54 m	21.19 m	−3.2%	30.44 m	31.36 m	−3.0%	90.47 m	91.89 m	−1.6%

Table 4 Comparison of numerical solution and analytical solution of water head on tunnel structure (H_f = 150 m)

	L_1			L_2			L_3		
	Analytical solution	Numerical solution	Relative error	Analytical solution	Numerical solution	Relative error	Analytical solution	Numerical solution	Relative error
X^+	39.05 m	38.82 m	0.6%	53.76 m	54.41 m	−1.2%	143.94 m	144.95 m	−0.7%
X^+Y^+	39.19 m	38.37 m	2.1%	53.93 m	53.23 m	1.8%	144.12 m	141.96 m	1.5%
Y^+	39.57 m	37.43 m	5.4%	54.42 m	52.62 m	3.3%	144.62 m	141.15 m	2.4%
X^-Y^+	40.02 m	38.58 m	3.6%	55.07 m	53.91 m	2.1%	145.30 m	143.41 m	1.3%
X^-	40.24 m	39.88 m	0.9%	55.43 m	55.76 m	−0.6%	145.68 m	147.28 m	−1.1%
X^-Y^-	40.02 m	40.98 m	−2.4%	55.07 m	56.12 m	−1.9%	145.30 m	147.77 m	−1.7%
Y^-	39.57 m	41.27 m	−4.3%	54.42 m	56.27 m	−3.4%	144.62 m	148.67 m	−2.8%
X^+Y^-	39.19 m	39.70 m	−1.3%	53.93 m	55.17 m	−2.3%	144.12 m	146.13 m	−1.4%

Table 5 Comparison of numerical solution and analytical solution of water head on tunnel structure (H_f = 200 m)

	L_1			L_2			L_3		
	Analytical solution	Numerical solution	Relative error	Analytical solution	Numerical solution	Relative error	Analytical solution	Numerical solution	Relative error
X^+	54.24 m	51.53 m	0.5%	73.89 m	73.29 m	0.8%	194.14 m	192.00 m	1.1%
X^+Y^+	54.37 m	53.66 m	1.3%	73.93 m	72.97 m	1.3%	194.18 m	194.46 m	1.4%
Y^+	54.74 m	53.32 m	2.6%	74.06 m	72.21 m	2.5%	194.31 m	188.86 m	2.9%
X^-Y^+	55.18 m	54.08 m	2.0%	74.26 m	73.07 m	1.6%	194.52 m	192..19 m	1.2%
X^-	55.39 m	54.95 m	0.8%	75.52 m	74.76 m	1.0%	194.84 m	196.01 m	−0.6%
X^-Y^-	55.18 m	55.21 m	−0.7%	74.26 m	75.00 m	−1.0%	194.52 m	196.46 m	−1.0%
Y^-	54.74 m	56.21 m	−2.7%	74.06 m	75.31 m	1.7%	194.31 m	197.81 m	−1.8%
X^+Y^-	54.37 m	55.02 m	−1.5%	73.93 m	75.11 m	1.6%	194.18 m	196.51 m	1.2%

in the Y^+ direction than the analytical solution. Combined with practical experience, the authors deem these deviations are generated owing to taking the gravity of water into account in the course of simulation and can be neglected. It notes that the numerical simulation generally consumes high costs and lots of time in modeling and computing and completes with the help of professional software. Especially for different engineering cases of geometry and boundary, such as the thickness of tunnel lining, the distance between tunnel and fault, and so on, the simulation modelling has been built once more. To sum up, the analytical method of hydraulic head on tunnel structure acquired by the virtual image technique in this paper can serve as a reasonable way in preliminary design, which clearly expresses the mechanical influence process and can satisfy the actual engineering accuracy required.

Parametric analysis

An extensive parametric analysis is conducted to investigate the performance on the hydraulic head at the key positions of the tunnel structure, including the primary lining, secondary lining and grouting ring on tunnel structure. The influencing factors include the magnitude of the hydraulic head, the distance between the fault and the tunnel centerline, the variation of water discharge after the lining drainage ditch installed and the fault dip. The proposed analysis may be useful for engineers to conduct a related preliminary assessment.

In the practical project, the far-field head and the head of water-bearing fault generally positively correlated with the varying supply of the groundwater or surface water. Hence, the parametric analysis of the magnitude of the water-bearing fault head is carried out by considering the ratio of the far-field head and water-bearing fault head being in steady.

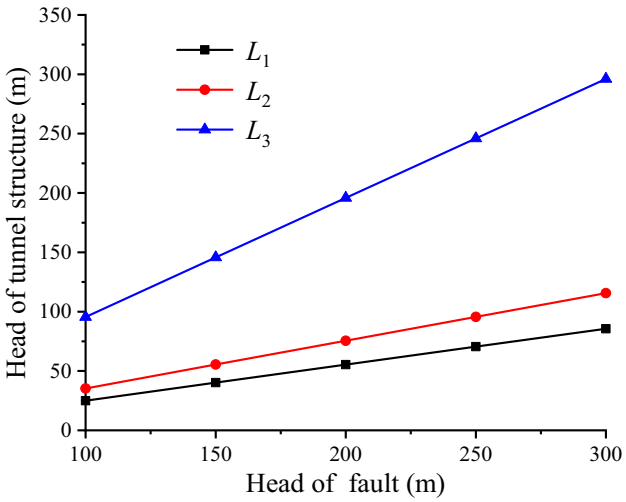

Fig. 12 Influence of water-bearing fault head on tunnel structure head

Influence of fault head on tunnel structure head

To investigate the performance of the head of the water-bearing fault on the tunnel structure before the drainage ditch installed, the distance from the fault to the tunnel centerline d is set 10 m, while the fault head H_f employs 100 m, 150 m, 200 m, 250 m and 300 m.

Figure 12 is plotted to analyze the influence of the water-bearing fault head on L_1, L_2 and L_3 of tunnel structure. As demonstrated in Fig. 12, the hydraulic head on the tunnel structure increases approximately linearly with the increase of the head of the water-bearing fault. Compared with the water head on L_3, the head on L_1 and L_2 increases much more slowly as the fault head rises owing to the larger permeability coefficient of the grouting ring. In addition, the trend between the head on the tunnel structure and the fault head remains consistent with that described in Fig. 12, as the spacing between the tunnel centerline and the fault d varies.

To investigate the influence of the head of water-bearing fault on the uneven distribution of the head on the tunnel structure, the magnitude of hydraulic head at any locations on the tunnel structure is obtained through combining Eqs. (50), (56), (61) and (66), as $H = f(r, \theta)$. When the fault dip reaches to 0°, the farthest water head from the fault ($\theta = \pi$), becomes the smallest under the condition that the distance from the tunnel centerline r is certain. Therefore, this paper presents the coefficient of head difference between each point on the same radius and the minimum head to explore the performance of fault head on the uneven distribution of hydraulic head on the tunnel structure. The head difference can be expressed as

$$H_d = f(r, \theta) - f(r, \pi). \tag{68}$$

Figure 13 plots the radar charts derived by analyzing the position head difference H_d of four cases, in which the heads of the water-bearing fault are set as 50 m, 75 m, 100 m and 200 m, respectively; and the distances between the fault and the tunnel center are $d = 10$ m. Results in Fig. 13 illustrate that the hydraulic head difference on the tunnel presents a transverse apple-shape form, in which the minimum value exists at the axis of 180°, while the maximum locates at the axis of 0°. Through comparisons of the water head difference

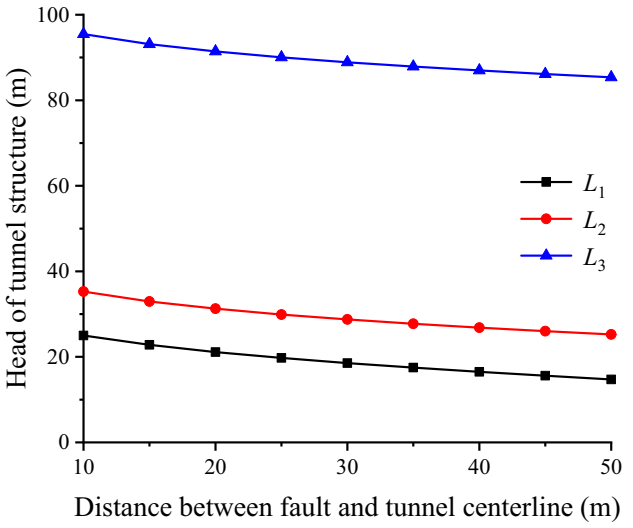

Fig. 14 Influence of distance between fault and tunnel on tunnel structure head

on the same circumference in Fig. 13, it is demonstrated that the hydraulic head difference will decrease as the head of water-bearing fault increases. Meanwhile, the uneven

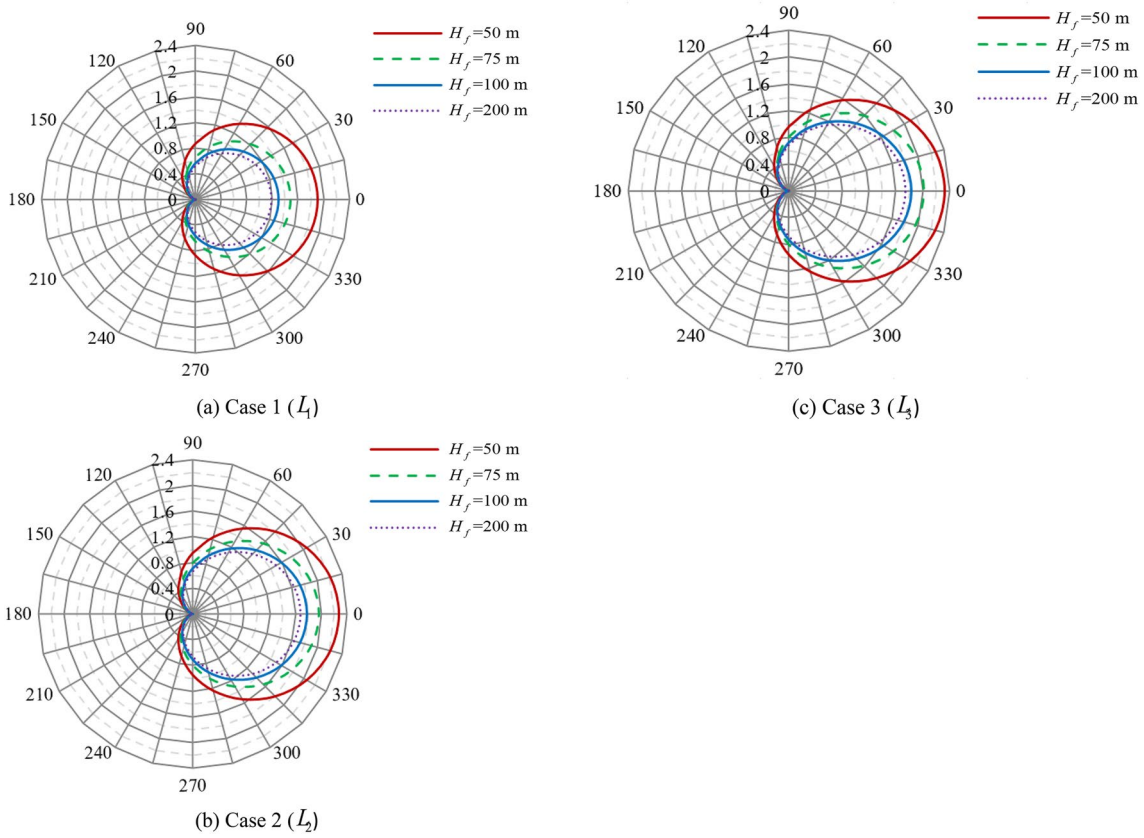

Fig. 13 Influence of fault head on uneven distribution of tunnel structure head. (**a**) Case 1 (L_1), (**b**) Case 2 (L_2), (**c**) Case 3 (L_3)

distribution of head on the structure is evidently weakened with the increase of head of water-bearing fault.

Influence of distance between fault and tunnel centerline on tunnel structure head

Figure 14 shows the plots for the performance of the distance between fault and tunnel on the magnitude of the tunnel structure head, in which the distances are set as 10 m, 15 m, 20 m, 25 m, 30 m, 35 m, 40 m, 45 m and 50 m, respectively, while the head of water-bearing fault H_f remains 100 m. Figure 14 is plotted for the average hydraulic head on L_1, L_2 and L_3. It can be observed that the head on tunnel structure decreases slightly along with the increase of the distance between the fault and the tunnel centerline. In addition, the heads on structure share a resembling decreasing trend. As the spacing increases from 10 to 50 m, the heads at different locations decrease roughly 7 m.

Figure 15 is plotted for the head difference H_d on the tunnel structure with the spacing between the fault and the tunnel centerline. The distances d are set as 10 m, 20 m, 30 m, and 40 m, respectively, while the head of fault H_f is 100 m. As revealed in Fig. 15, it demonstrates that the uneven distribution of hydraulic head on the structure is weakened as the distance between the fault and the tunnel centerline increases.

Influence of lining drainage ditch on tunnel structure head

In practical engineering, drainage ditches are usually installed on the tunnel lining to reduce the external water pressure on the lining. The water discharge of the tunnel will obviously increase by a wide margin after drainage ditches are installed. The distribution of the hydraulic head on the tunnel structure can be performed by the analytical solution in this paper when the tunnel discharge changes due to the setting of drainage ditches, under the condition of certain fault head and far-field head.

Figure 16 illustrates the performance of tunnel discharge on hydraulic head on L_1, L_2 and L_3. The head of fault H_d is

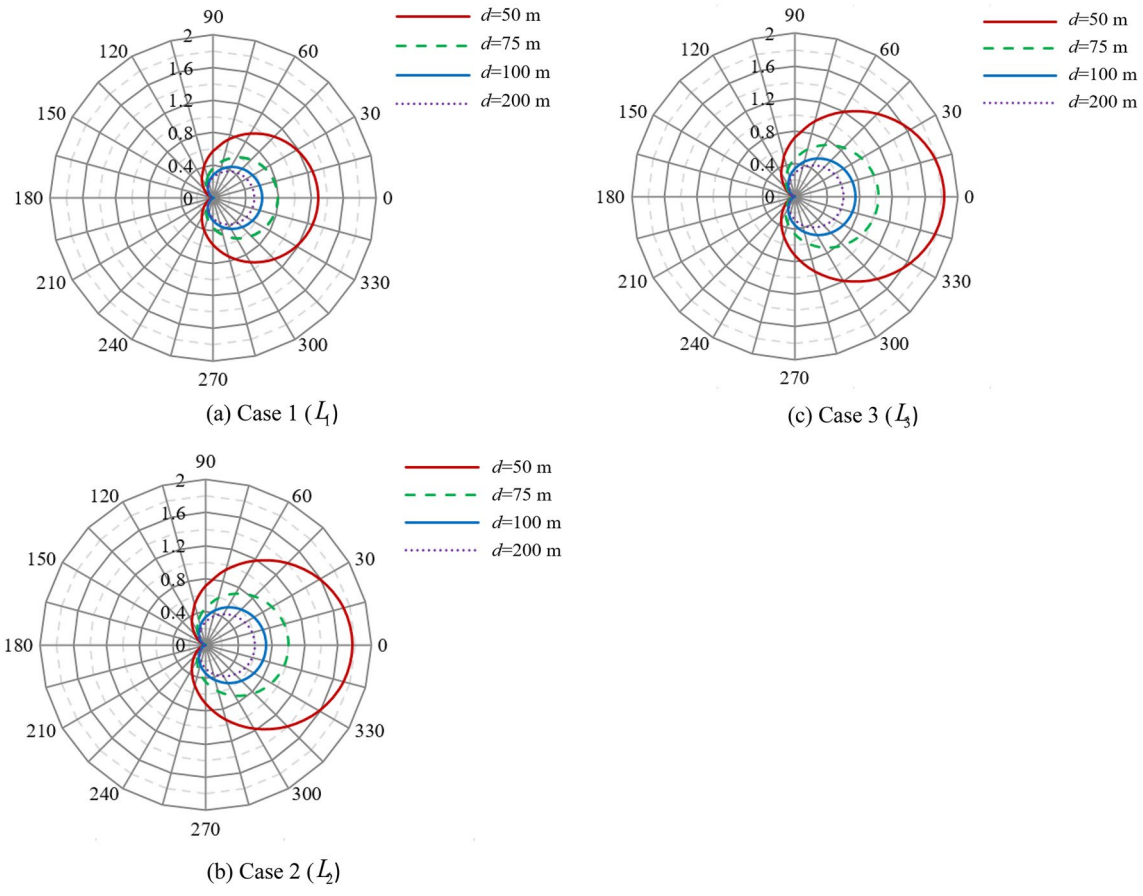

Fig. 15 Influence of distance between fault and tunnel on uneven distribution of tunnel structure head. (**a**) Case 1 (L_1), (**b**) Case 2 (L_2), (**c**) Case 3 (L_3)

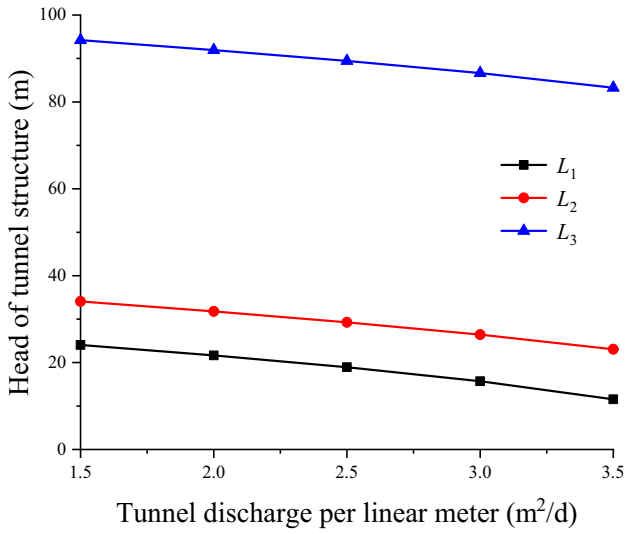

Fig. 16 Influence of tunnel discharge per linear meter on tunnel structure head

taken as 100 m and the distance d is set 10 m. The water discharge of linear meter of tunnel is 1.47 m^2/d through the analytical solution in this paper taking no drainage ditches into account. However, the discharge of tunnel will change after the drainage ditches are set. Hence, this section sets five cases of discharge per linear meter to conduct the performance on the magnitude of head on the tunnel structure and uneven distribution. The cases are 1.47 m^2/d, 2 m^2/d, 2.5 m^2/d, 3 m^2/d and 3.5 m^2/d, respectively. From Fig. 16, it shows that the tunnel discharge remarkably enlarges owing to the lining drainage ditch installed, resulting into the hydraulic head on the tunnel structure significantly weakened.

Figure 17 displays the influence of the uneven distribution on the tunnel structure due to tunnel discharge, which plots the head difference H_d on the tunnel structure under different conditions of discharge. As the water discharge increases, the hydraulic head on tunnel structure gradually decreases, while the uneven distribution of the head

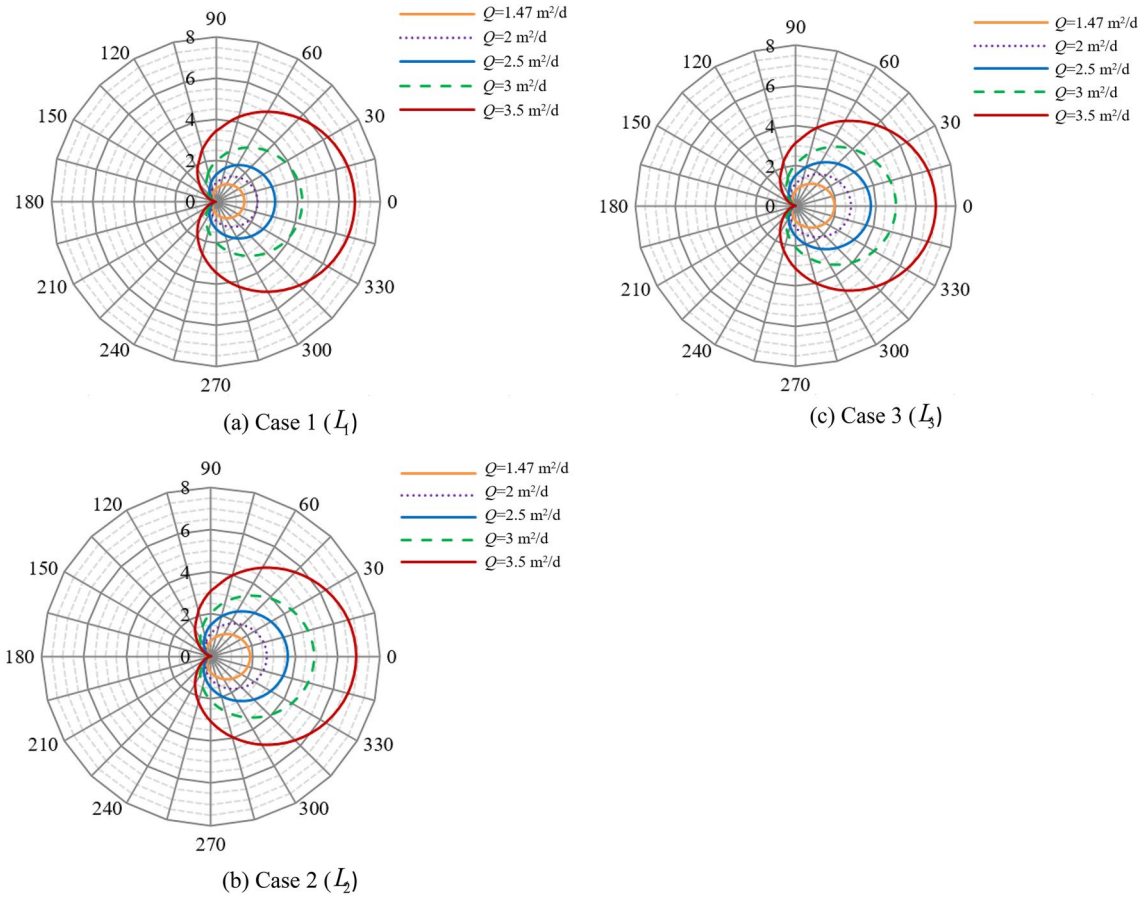

Fig. 17 Influence of discharge per linear meter on uneven distribution of tunnel structure head. (**a**) Case 1 (L_1), (**b**) Case 2 (L_2), (**c**) Case 3 (L_3)

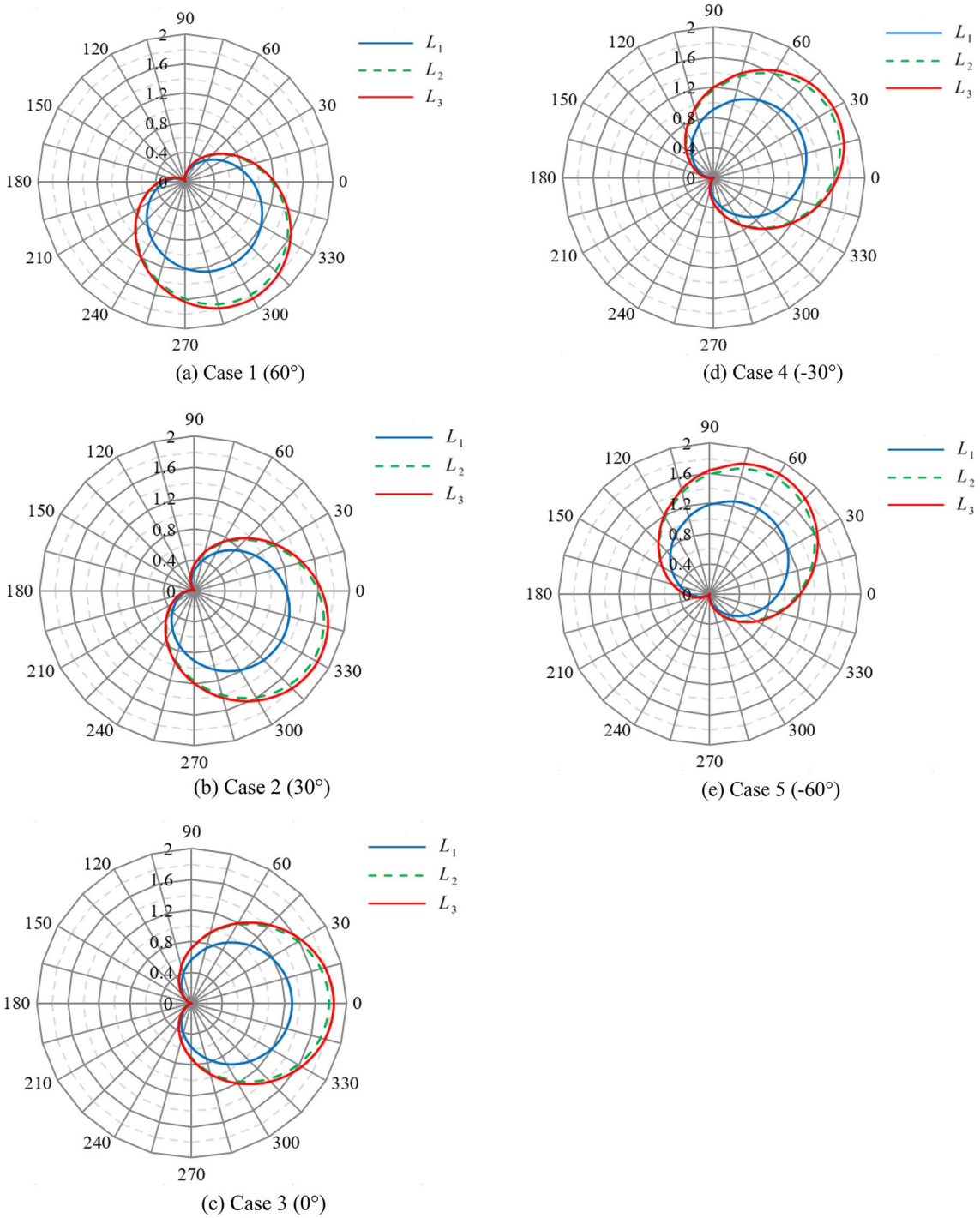

Fig. 18 Influence of fault dip angle on uneven distribution of tunnel structure head. (**a**) Case 1 (60°). (**b**) Case 2 (30°). (**c**) Case 3 (0°). (**d**) Case 4 (− 30°). (**e**) Case 5 (− 60°)

tends to rise up. When the discharge per linear meter of the tunnel is 3.5 m^2/d, the maximum head difference H_d at the same distance from the tunnel centerline will expand to approximately 7 m. In addition, the results of Figs.16 and 17 demonstrate the location of the tunnel structure has limited influence on the head difference.

Influence of fault dip on tunnel structure head

To investigate the influence of the fault dip on the uneven distribution of the tunnel head, the concerned parameters are set as, the head of fault H_d 100 m, and the distance d 10 m, before the lining drainage ditch is installed. The performance

on the uneven distribution of the hydraulic head is investigated through different dip angles of the fault, which is set on the right side of the tunnel. The angle of the vertical fault is assumed 0°, and the dip angle is stipulated positive in the clockwise direction and is negative in the anticlockwise direction. This section presents four cases, in which the dips are set as 30°, 60°, −30° and −60°. Figure 18 is plotted to investigate the influence of fault angle on uneven distribution of head, and the results show that the fault dip places significant influence on the uneven distribution of the hydraulic head on the tunnel structure. The distribution of apple-shape head difference is rotated a certain angle as the fault dip varies. Moreover, the line between the maximum and minimum values of head on the tunnel structure at the same circumference will always be vertical to the fault.

Conclusions

In this paper, the tunnel discharge induced by a far-field head and a fault head is investigated based on an actual mountain tunnel adjacent to a water-bearing fault in water-rich region. This paper presents an efficient and reliable way to evaluate the hydraulic head on tunnel structure due to the influence of fault head through the virtual image method and the complex variable method. The close-form analytical solution is then checked with the classical Harr solution and numerical solution implemented in this work, and fine alignments are obtained. Moreover, the paper proposes the influence of sensitive parameters on the value of hydraulic head and uneven distribution. The major outcomings are as follows:

The size of the fault head and the distance between the fault and the tunnel centerline have significant influence on the size and uneven distribution of the hydraulic head on the tunnel structure owing to the water-bearing fault adjacent to the tunnel. The head on the tunnel structure maintains a positive correlation with the water-bearing fault head; meanwhile, the uneven distribution weakens. The hydraulic head and the uneven distribution decrease with the increase of the distance between the fault and the tunnel centerline.

The interesting point in this study is achieving the relevant analytical solutions for not only the influence of vertical fault adjacent to the tunnel but also the fault with an inclined dip angle, which improves the engineering applicability of the presented method. The uneven distribution presents an apple-shape form, while the distribution of the hydraulic head may be affected by the fault dip. The shape will rotate a little with different fault dips. However, the line between the maximum and minimum values of the head on the tunnel structure is always vertical to the fault under diverse cases. The tunnel discharge significantly increases by installing lining drainage ditches. The increase of water discharge may effectively reduce the head on the tunnel structure as the uneven distribution of hydraulic head on the tunnel structure increases.

The core work of this paper is to obtain the water head and head distribution on the tunnel structure by analyzing the magnitude of head considering the influences of fault geology so as to introduce the theoretical basis for the response of the lining in the course of tunnel excavation and put forward reasonable reinforcement measures. Furthermore, the above-mentioned aim is accomplished by the complex variable analytical method and the virtual image method. It is interesting achievement in developing the analytical methods to simulate the tunnel–fault interaction mechanisms. However, the major limitations of the method presented in this paper stem from the existing assumptions of isotropic and homogeneous behavior of surrounding rock and tunnel, which is in contradiction with the actual engineering. Furthermore, the coupling between the fault head and the far-field head is not taken into account in this paper. With the improvement of analytical methods and the increase of measured data, further research will be adopted more realistic hypothesis. Consequently, the relevant studies on this subject are still required to evaluate the head distribution on tunnel structure adjacent to water-bearing fault more effectively.

Appendix A: Derivations related to Darcy's law

Darcy did a lot of seepage experiments and obtained the seepage law, known as Darcy's law, whose form is as follows:

$$Q = kA\frac{H_1 - H_2}{L} = kAJ, \tag{A-1}$$

where Q is the seepage discharge; k is the permeability coefficient (hydraulic conductivity coefficient); H_1–H_2 is the Water head difference; L is the distance of sections; J is the hydraulic gradient.

The relationship between seepage discharge and seepage velocity is as follows:

$$v = \frac{Q}{A}, \tag{A-2}$$

where v is the seepage velocity (Darcy seepage).

Combine Eq. (A-1) with Eq. (A-2), it is derived as

$$v = kJ. \tag{A-3}$$

If the Darcy's law is applied to two-dimensional or three-dimensional groundwater movement, the hydraulic gradient

J is not a constant and should be expressed in differential form as follows:

$$v = -k\frac{dH}{ds}, \tag{A-4}$$

where $-\frac{dH}{ds}$ is the hydraulic gradient at any point along the streamline. In rectangular coordinates, Eq. (4) can be expressed as

$$v_x = -k\frac{\partial H}{\partial x} \tag{A-5}$$

$$v_y = -k\frac{\partial H}{\partial y} \tag{A-6}$$

$$v_z = -k\frac{\partial H}{\partial z} \tag{A-7}$$

Acknowledgements The authors would like to thank the researchers for their contributions to the analytical solutions. The authors also thank Mr. Zhongteng Wu for his contribution to revise and improve this paper. The authors acknowledge the financial support provided by National Natural Science Foundation of China for General Program (Nos. 41772331 and 41977247), and the Opening Fund of Key Laboratory of Geohazard Prevention of Hilly Mountains, Ministry of Natural Resources (Fujian Key Laboratory of Geohazard Prevention, No. FJKLGH2020K004), and the Project of State Key Laboratory Fund for State Key Laboratory of Geohazard Prevention and Geoenvironment Protection (No. SKLGP2015K015).

References

Arjoni P, Jeong JH, Kim CY, Park KH (2009) Effect of drainage conditions on porewater pressure distributions and lining stresses in drained tunnels. Tunn Undergr Space Technol 24(4):376–389. https://doi.org/10.1016/j.tust.2008.10.006

Bear J (1972) Dynamics of fluids in porous media. Dover Publ Inc, New York

Bian K, Xiao M, Chen JT (2009) Study on coupled seepage and stress fields in the concrete lining of the underground pipe with high water pressure. Tunn Undergr Space Technol 24(3):287–295. https://doi.org/10.1016/j.tust.2008.10.003

Bobet A (2003) Effect of pore water pressure on tunnel support during static and seismic loading. Tunn Undergr Space Technol 18(4):377–393. https://doi.org/10.1016/s0886-7798(03)00008-7

Boultbee N, Robson O, Moalli S, Humphries R (2018) Upper Lillooet River hydroelectric project: the challenge of constructing a power tunnel for run-of river hydro projects in mountainous British Columbia. Eng 4(2):260–266. https://doi.org/10.1016/j.eng.2017.09.003

Chen CX, Hu LT, Wang XS (2006) Analysis of steady ground water flow toward wells in a confined-unconfined aquifer. Groundwater 44(4):609–612. https://doi.org/10.1111/j.1745-6584.2006.00170.x

Cheng P, Zhao LH, Luo ZB, Li Q, Deng X, Peng WQ (2019) Analytical solution for the limiting drainage of a mountain tunnel based on area-well theory. Tunn Undergr Space Technol 84(2):22–30. https://doi.org/10.1016/j.tust.2018.10.014

Childs C, Manzocchi T, Walsh JJ, Bonson CG, Nical A, Schöpfer MPJ (2009) A geometric model of fault zone and fault rock thickness variations. J Struct Geol 31(2):117–127. https://doi.org/10.1016/j.jsg.2008.08.009

Deng MJ (2018) Challenges and thoughts on risk management and control for the group construction of a super-long tunnel by TBM. Eng 4(1):112–122. https://doi.org/10.1016/j.eng.2017.07.001

Dong XJ, Karrech A, Basarir H, Elchalakani M, Qi CC (2018b) Analytical solution of energy redistribution in rectangular openings upon in-situ rock mass alteration. Int J Rock Mech Min Sci 106(4):74–83. https://doi.org/10.1016/j.ijrmms.2018.04.014

Dong XJ, Karrech A, Qi CC, Elchalakani M, Basarir H (2019) Analytical solution for stress distribution around deep lined pressure tunnels under the water table. Int J Rock Mech Min Sci 123(9):104124. https://doi.org/10.1016/j.ijrmms.2019.104124

Dong XJ, Karrech A, Basarir H, Elchalakani M, Qi CC (2020) Closed-form folution to the poromechanics of deep arbitrary-shaped openings subjected to rock mass alteration. Int J Geomech 20(12):04020223. https://doi.org/10.1061/(ASCE)GM.1943-5622.0001875

Dong XJ, Karrech A, Basarir H, Elchalakani M (2018a) Extended finite element modelling of fracture propagation during in-situ rock mass alteration. In Proc., 52nd US Rock Mechanics/Geomechanics Symp., 1–8. Alexandria, VA: American Rock Mechanics Association.

Fahimifar A, Zareifard MR (2009) A theoretical solution for analysis of tunnels below groundwater considering the hydraulic–mechanical coupling. Tunn Undergr Space Technol 24(6):634–646. https://doi.org/10.1016/j.tust.2009.06.002

Fang Y, Guo JN, Grasmick J, Mooney M (2016) The effect of external water pressure on the liner behavior of large cross-section tunnels. Tunn Undergr Space Technol 60(11):80–95. https://doi.org/10.1016/j.tust.2016.07.009

Fernandez G, Moon J (2010) Excavation-induced hydraulic conductivity reduction around a tunnel-Part 2: verification of proposed method using numerical modeling. Tunn Undergr Space Technol 25(5):567–574. https://doi.org/10.1016/j.tust.2010.04.001

Girinskii NK (1946) Generalization of some solutions for wells to more complicated natural conditions (in Russian). Rep USSR Acad Sci 54(3):18–25

Harr ME (1962) Groundwater and seepage. McGraw-Hill, New York

Huang Y, Fu ZM, Chen J, Zhou ZF, Wang JG (2015) The external water pressure on a deep buried tunnel in fractured rock. Tunn Undergr Space Technol 48(4):58–66. https://doi.org/10.1016/j.tust.2015.02.003

Huang F, Wu CZ, Ni PP, Wan GP, Zheng AC, Jang BA, Karekal S (2020) Experimental analysis of progressive failure behavior of rock tunnel with a fault zone using non-contact DIC technique. Int J Rock Mech Min Sci 132(8):104355. https://doi.org/10.1016/j.ijrmms.2020.104355

Hwang J, Lu C (2007) A semi-analytical method for analyzing the tunnel water inflow. Tunn Undergr Space Technol 22(1):39–46. https://doi.org/10.1016/j.tust.2006.03.003

Ikuma M (2005) Maintenance of the undersea section of the Seikan Tunnel. Tunn Undergr Space Technol 20(2):143–149. https://doi.org/10.1016/j.tust.2003.10.001

Jeon S, Kim J, Seo Y, Hong C (2004) Effect of a fault and weak plane on the stability of a tunnel in rock-a scaled model test and numerical analysis. Int J Rock Mech Min Sci 41(5):658–664. https://doi.org/10.1016/j.ijrmms.2004.03.115

Kargar AR (2019) An analytical solution for circular tunnels excavated in rock masses exhibiting viscous elastic-plastic behavior. Int J Rock Mech Min Sci 124(12):104128. https://doi.org/10.1016/j.ijrmms.2019.104128

Kargar AR, Babanouri HH (2020) Time-dependent analysis of stress components around lined tunnels with circular configuration considering tunnel advancing rate effects. Int J Rock Mech Min Sci 133(9):104422. https://doi.org/10.1016/j.ijrmms.2020.104422

Kargar AR, Rahmannejada R, Hajabasib MA (2015) The stress state around lined non-circular hydraulic tunnels below the water table using complex variable method. Int J Rock Mech Min Sci 78(9):207–216. https://doi.org/10.1016/j.ijrmms.2015.04.005

Kim HJ, Eisenstein Z (2006) Prediction of tunnel lining loads using correction factors. Eng Geol 85(3):302–312. https://doi.org/10.1016/j.enggeo.2006.03.001

Kim YG, Han BH, Lee SB, Kim ET (2011) A case study of collapse and reinforcement for large span waterway tunnel at thrust fault zone. J Korean Soc Rock Mech 21(4):251–263. https://doi.org/10.7474/tus.2011.21.4.251

Kolymabas D, Wagner P (2007) Groundwater ingress to tunnels—the exact analytical solution. Tunn Undergr Space Technol 22(1):23–27. https://doi.org/10.1016/j.tust.2006.02.001

Lai JX, Wang XL, Qiu JL, Chen JX, Hu ZN, Hao W (2018) Extreme deformation characteristics and countermeasures for a tunnel in difficult grounds in southern Shaanxi. China Environ Earth Sci 77(10):706. https://doi.org/10.1007/s12665-018-7888-2

Lee IM, Nam SW (2004) Effect of tunnel advance rate on seepage forces acting on the underwater tunnel face. Tunn Undergr Space Technol 19(3):273–281. https://doi.org/10.1016/j.tust.2003.11.005

Lee IM, Lee JS, Nam SW (2004) Effect of seepage force on tunnel face stability reinforced with multistep pipe grouting. Tunn Undergr Space Technol 19(6):551–565. https://doi.org/10.1016/j.tust.2004.01.003

Lee SW, Jung JW, Nam SW, Lee IM (2007) The influence of seepage forces on ground reaction curve of circular opening. Tunn Undergr Space Technol 22(1):28–38. https://doi.org/10.1016/j.tust.2006.03.004

Li HZ, Low BK (2010) Reliability analysis of circular tunnel under hydrostatic stress field. Comput Geotech 7(1):50–58. https://doi.org/10.1016/j.compgeo.2009.07.005

Lin CG, Wu SM, Xia TD, Gao GY (2014) Observed response of a shield-driven tunnel to fluctuations in river stage. Environ Earth Sci 73(11):6311–6322. https://doi.org/10.1007/s12665-014-3853-x

Liu XZ, Li XF, Sang YL, Lin LL (2015) Experimental study on normal fault rupture propagation in loose strata and its impact on mountain tunnels. Tunn Undergr Space Technol 49(6):417–245. https://doi.org/10.1016/j.tust.2015.05.010

Liu FS (2012) Seepage studies of tunnel in water-enriched region based on fluid-solid coupling theory and complex analysis [Ph. D Thesis]. Guangdong: South China University of Technology. (in Chinese)

Luo ZJ, Zhang YY, Wu YX (2008) Finite element numerical simulation of three-dimensional seepage control for deep foundation pit dewatering. J Hydro 20(10):596–602. https://doi.org/10.1016/s1001-6058(08)60100-6

Lyu HM, Shen SL, Zhou AN, Chen KL (2020) Calculation of pressure on the shallow-buried twin-tunnel in layered strata. Tunn Undergr Space Technol 103(9):103465. https://doi.org/10.1016/j.tust.2020.103465

Miura K (2003) Design and construction of mountain tunnels in Japan. Tunn Undergr Space Technol 18(2):115–126. https://doi.org/10.1016/s0886-7798(03)00038-5

Moon J, Jeong S (2010) Effect of highly pervious geological features on ground-water flow into a tunnel. Eng Geol 117(3):207–216. https://doi.org/10.1016/j.enggeo.2010.10.019

Nam SW, Bobet A (2006) Liner stresses in deep tunnels below the water table. Tunn Undergr Space Technol 21(6):626–635. https://doi.org/10.1016/j.tust.2005.11.004

Park KH, Lee JG, Owatsiriwong A (2008) Seepage force in a drained circular tunnel: an analytical approach. Can Geo J 45(3):432–436. https://doi.org/10.1139/t07-113

Patterson FW, Clinch RL, McCaig IW (1957) Design of large pressure conduits in rock. J Power Div 83(6):1–30

Shen YS, Gao B, Yang XM, Tao SG (2014) Seismic damage mechanism and dynamic deformation characteristic analysis of mountain tunnel after Wenchuan earthquake. Eng Geol 180(8):85–98. https://doi.org/10.1016/j.enggeo.2014.07.017

Shin JH, Potts DM, Zdravkovic L (2005) The effect of pore-water pressure on NATM tunnel linings in decomposed granite soil. Can Geotech J 42(6):1585–1599. https://doi.org/10.1139/t05-072

Shin HS, Youn DJ, Chae SE, Shin JH (2009) Effective control of pore water pressures on tunnel linings using pin-hole drain method. Tunn Undergr Space Technol 24(5):555–561. https://doi.org/10.1016/j.tust.2009.02.006

Snow DT (1969) Anisotropic permeability of featured media. Water Resour Res 5(6):1273–1289. https://doi.org/10.1029/wr005i006p01273

Tan YQ, Smith JV, Li CQ, Currell M, Wu YF (2018) Predicting external water pressure and cracking of a tunnel lining by measuring water inflow rate. Tunn Undergr Space Technol 71(2):115–125. https://doi.org/10.1016/j.tust.2017.08.015

Vaughan EW (1956) Steel linings for pressure shafts in solid rocks. J Power Div 82(2):1–40

Wang XY, Tan ZS, Wang MS, Zhang M, Ming HF (2008) Theoretical and experimental study of external water pressure on tunnel lining in controlled drainage under high water level. Tunn Undergr Space Technol 23(5):552–560. https://doi.org/10.1016/j.tust.2007.10.004

Wang YC, Jing HW, Su HJ, Xie JY (2016a) Effect of a fault fracture zone on the stability of tunnel-surrounding rock. Int J Geomech 17(6):04016135. https://doi.org/10.1061/(asce)gm.1943-5622.0000837

Wang YC, Jing HW, Su HJ, Xie JY (2016b) Numerical study on the tunnel instability in fault zone: a case study of Wuzhuling Tunnel in China. Proc GeoChina ASCE GSP. https://doi.org/10.1061/9780784480038.028

Wu J, Li SC, Xu ZH, Huang X, Xue YG, Wang ZC, Li LP (2017) Flow characteristics and escape-route optimization after water inrush in a backward-excavated karst tunnel. Int J Geomech 17(4):1–16. https://doi.org/10.1061/(asce)gm.1943-5622.0000787

Wu YX, Lyu HM, Shen SL, Arulrajah A (2018) Geological and hydrogeological environment in Tianjin with potential geohazards and groundwater control during excavation. Environ Earth Sci 77(5):392. https://doi.org/10.1007/s12665-018-7555-7

Wu J, Li SC, Xu ZH, Zhao J (2019) Determination of required rock thickness to resist water and mud inrush from karst caves in front of tunnel face under earthquake action. Tunn Undergr Space Technol 85(3):43–55. https://doi.org/10.1016/j.tust.2018.11.048

Xie YY, Hu ZR, Lu GJ, Zhang XM, Zhao CM, Cheung LK (2013) Instant numerical simulation research on fire ventilation in extra-long highway tunnel in Zhongnanshan section of Qinlin mountains. Pro Eng 52:468–474. https://doi.org/10.1016/j.proeng.2013.02.170

Ye F, He C, Wang SM, Zhang JL (2012) Landscape design of mountain highway tunnel portals in China. Tunn Undergr Space Technol 29(5):52–68. https://doi.org/10.1016/j.tust.2012.01.001

Yoo C (2005) Interaction between tunneling and groundwater-numerical investigation using three dimensional stress-pore pressure coupled analysis. J Geo Geoen Eng 131(2):240–250. https://doi.org/10.1061/(asce)1090-0241(2005)131:2(240)

Young W, Falkiner RH (1966) Some design and construction features of cruachan pumped storage project. Proc Inst Civil Eng 35(3):407–450. https://doi.org/10.1680/iicep.1966.8725

Yu C, Deng SC, Li HB, Li JC, Xia X (2013) The anisotropic seepage analysis of water-sealed underground oil storage caverns. Tunn Undergr Space Technol 38(9):26–37. https://doi.org/10.1016/j.tust.2013.05.003

Zhang ZQ, Chen FF, Li N, Swoboda G, Liu NF (2017) Influence of fault on the surrounding rock stability of a tunnel: Location and thickness. Tunn Undergr Space Technol 61(1):1–11. https://doi.org/10.1016/j.tust.2016.09.003

Zhang N, Shen SL, Zhou AN, Arulrajah A (2018a) Tunneling induced geohazards in mylonitic rock faults with rich groundwater: a case study in Guangzhou. Tunn Undergr Space Technol 74(4):262–272. https://doi.org/10.1016/j.tust.2017.12.021

Zhang XP, Jiang YJ, Sugimoto SH (2018b) Seismic damage assessment of mountain tunnel: a case study on the Tawarayama tunnel due to the 2016 Kumamoto Earthquake. Tunn Undergr Space Technol 71(1):138–148. https://doi.org/10.1016/j.tust.2017.07.019

Zhao Y, Li PF, Tian SM (2013) Prevention and treatment technologies of railway tunnel water inrush and mud gushing in China. J Rock Mech Geo Eng 5(6):468–477. https://doi.org/10.1016/j.jrmge.2013.07.009

Zhao K, Janutolo M, Barla G, Chen GX (2014) 3D simulation of TBM excavation in brittle rock associated with fault zones: the Brenner exploratory tunnel case. Eng Geol 181(10):93–111. https://doi.org/10.1016/j.enggeo.2014.07.002

Zhao K, Chen WZ, Yang DS, Zhao WS, Wang SY, Song WP (2019) Mechanical tests and engineering applicability of fibre plastic concrete used in tunnel design in active fault zones. Tunn Undergr Space Technol 88(6):200–208. https://doi.org/10.1016/j.tust.2019.03.009

Zhu HH, Yan JX, Liang WH (2019) Challenges and development prospects of ultra-long and ultra-deep mountain tunnels. Eng 5(3):384–392. https://doi.org/10.1016/j.eng.2019.04.009